

Front page

Title:

A leaf-level biochemical model simulating the introduction of C₂ and C₄ photosynthesis in C₃ rice: gains, losses and metabolite fluxes

Authors and addresses:

Chandra Bellasio^{1-3*} and Graham D Farquhar¹

¹Research School of Biology, Australian National University, Acton, ACT, 2601 Australia;

²University of the Balearic Islands 07122 Palma, Illes Balears, Spain;

³Trees and Timber institute, National Research Council of Italy, 50019 Sesto Fiorentino (Florence).

Correspondence details:

chandra.bellasio@anu.edu.au

Word counts:

Summary: 200; Introduction to Conclusion: 6595.

Number of tables:

1

Figures:

6 (5 in colour).

Supporting information:

File 1: 25 pages, 10 notes, 9 figures, and 3 tables.

File 2: The model, coded in Excel, made freely available.

2 **A leaf-level biochemical model simulating the introduction of C₂ and** 3 **C₄ photosynthesis in C₃ rice: gains, losses and metabolite fluxes**

4 Chandra Bellasio^{1-3*} and Graham D Farquhar¹

5 ¹Research School of Biology, Australian National University, Acton, ACT, 2601 Australia;

6 ²University of the Balearic Islands 07122 Palma, Illes Balears, Spain;

7 ³Trees and Timber institute, National Research Council of Italy, 50019 Sesto Fiorentino (Florence).

8 *Correspondence: chandra.bellasio@anu.edu.au

9 **Summary:**

- 10 • This work aims at developing an adequate theoretical basis for comparing assimilation of the
11 ancestral C₃ pathway with CO₂ concentrating mechanisms (CCM) that have evolved to reduce
12 photorespiratory yield losses.
- 13 • We present a novel model for C₃, C₂, C₂+C₄ and C₄ photosynthesis simulating assimilatory me-
14 tabolism, energetics, and metabolite traffic at the leaf-level. It integrates a mechanistic de-
15 scription of light reactions to simulate ATP and NADPH production, and a variable engage-
16 ment of cyclic electron flow. The analytical solutions are compact and thus suitable for larger
17 scale simulations. Inputs were derived with a comprehensive gas exchange experiment.
- 18 • We show trade-offs in the operation of C₄ that are in line with ecophysiological data. C₄ has
19 the potential to increase assimilation over C₃ at high temperatures and light intensities, but this
20 benefit is reversed under low temperatures and light.
- 21 • We apply the model to simulating the introduction of progressively complex levels of CCM
22 into C₃ rice, which feeds more than 3.5 billion people. Increasing assimilation will require con-
23 siderable modifications such as expressing the NDH complex and upregulating cyclic electron
24 flow, enlarging the bundle sheath, and expressing suitable transporters to allow adequate me-
25 tabolite traffic. The simpler C₂ rice may be a desirable alternative.

26 **Keywords**

27 Stomata, enzyme, light, limitation, C₂ shuttle, C₃-C₄ intermediate, photorespiration, bio-engi-
28 neering, synthetic biology, assimilation.

29 **Running title**

30 Simulating biochemical carbon concentrating mechanisms

31 Introduction

32 Carbon concentrating mechanisms (CCM; acronyms are listed in Table 1) are co-ordinated suites
33 of structural and biochemical modifications to ancestral C₃ photosynthesis. CCMs evolved to reduce
34 the magnitude of photorespiration, a complex process resulting in the release of previously fixed CO₂,
35 which incurs substantial energy costs to recycle by-products (Meyer & Griffiths, 2013). In plants,
36 CCMs have the form of biochemical cycles that increase the CO₂/O₂ ratio at the Rubisco catalytic
37 site, and are of two types: the 'C₂ shuttle' and the C₄ cycle. To operate a CCM, the photosynthetic pa-
38 renchyma is often differentiated into two cell types, although single-celled systems do exist (King *et*
39 *al.*, 2012): an external layer of mesophyll (M) and an internal layer of bundle sheath (BS) encircling
40 the vasculature (Lundgren *et al.*, 2014). The C₂ shuttle consists of the compartmentation of glycine
41 decarboxylase (GDC) activity in the BS, delivering CO₂ around Rubisco in the BS, using the pho-
42 torespiratory glycine produced in the M (Keerberg *et al.*, 2014). The C₄ cycle represents a further so-
43 phistication involving an energy dependent carboxylation-decarboxylation cycle. CO₂ is initially
44 fixed into a four-carbon (C₄) organic acid (OAA) in the M by phosphoenolpyruvate carboxylase
45 (PEPC), which after reduction (or transamination) diffuses to the BS where it is decarboxylated. If, on
46 the one hand, the C₄ cycle lowers the photorespiratory ATP demand, on the other it requires a con-
47 siderable amount of ATP (2 ATP per CO₂ pumped, for the NADP-ME subtype) for the regenera-
48 tion of phosphoenolpyruvate (Kanai & Edwards, 1999; Evans *et al.*, 2007; Bellasio, 2017). In
49 'C₂+C₄' species (Bellasio, 2017) the degree of PEPC engagement, and the extent of Rubisco compart-
50 mentation to the BS are intermediate and are species dependent (Monson & Moore, 1989). In C₄ spe-
51 cies, PEPC is fully engaged and CO₂ accumulates in the BS at concentrations that are 10- to 20-fold
52 greater than ambient, thereby saturating a fully compartmentalised Rubisco in the BS (von
53 Caemmerer & Furbank, 2003). The biochemical functions of the M and BS need to be separated by
54 a suitable distance (Jurić *et al.*, 2017). Across this space large fluxes of metabolites need to be ex-
55 changed, both through plasmodesmata (Osmond & Smith, 1976; Danila *et al.*, 2018), and through a
56 suite of chloroplast membrane transporters (Weber & von Caemmerer, 2010; Gowik *et al.*, 2011;
57 Schlüter *et al.*, 2016).

58 Quantifying the potential gains from operating a CCM has challenged physiologists for the last
59 50 years. Simple approaches have compared C₃ and C₄ plants, but the evolutionary traits of unre-
60 lated species can differ substantially, preventing the isolation of the effects of CCMs [reviewed in
61 Snaydon (1991) and Christin and Osborne (2014)]. For instance, in a large comparative experiment
62 Atkinson *et al.* (2016) found C₃ and C₄ grasses mainly differed in terms of leaf mass per area, rather
63 than net assimilation rate per unit leaf area, but Taylor *et al.* (2010) reported that a more limited set
64 of C₄ grasses had a 45 % higher assimilation rate than C₃ grasses. The comparison is further compli-
65 cated by the co-occurrence of acclimatory traits: Schmitt and Edwards (1981) reported that the ef-
66 fect of short and long term temperature acclimation was greater than any difference in assimilation

67 rate between maize and rice. Even in targeted comparisons between rice and the sympatric weed
68 *Echinochloa glabrescens* or crops such as maize, results were inconclusive (Sheehy, 2007;
69 Covshoff *et al.*, 2016). To quantify the benefit of operating a CCM it is therefore critical to compare
70 two plants in which all traits, other than the strength of the CCM, are equal.

71 For this hypothetical analysis, mathematical models are in principle the ideal tool. Heckmann *et*
72 *al.* (2013) found a smooth monotonic increase in assimilation for increasing levels of C₄ expression
73 in a C₃ background. This finding was directly dependent on the assumption of unlimited ATP, and
74 contrasts with the observation that C₄ plants are favoured only under high temperatures and light
75 intensities (Monteith, 1978; Pearcy & Ehleringer, 1984). Wu *et al.* (2017) compared predictions of
76 C₃ and C₄ models, but these were parameterised separately by curve fitting on representative C₃ and
77 C₄ crops, thereby replicating the unwanted coexistence of multiple traits present in nature within the
78 models. The light-limited model developed by von Caemmerer (2000) assumed a fixed stoichio-
79 metric conversion between electron transport and ATP production and is unsuitable for testing dif-
80 ferent levels of C₄ engagement because the C₄ cycle requires an increased ratio of ATP to NADPH,
81 which C₄ plants obtain by upregulating cyclic electron flow, CEF (Ishikawa *et al.*, 2016). Recently
82 Yin and Struik (2017) overcame some of these shortcomings, but biochemical processes were rela-
83 tively schematic, and as a result, metabolite exchange requirements have not been quantified.

84 The aims of this work were three-fold. Firstly, to develop the theoretical underpinnings of the
85 introduction of CCMs into C₃ crops at the leaf level; secondly, quantify the possible benefits and
86 trade-offs of CCMs if they were to be made operational in rice; and, finally, estimate realistic
87 fluxes to help define targets for expression of enzymes and transporters. Light-limited formulations
88 working under the assumption of limiting ATP or NADPH, as well as enzyme-limited formula-
89 tions, all valid for any photosynthetic type, are developed here. These are integrated with a mecha-
90 nistic description of photosynthetic light reactions, and with a biochemical and hydromechanical
91 model of stomatal behaviour. A gas-exchange experiment was used to inform the model. The re-
92 sults predict that introducing CCMs in C₃ metabolism under the current ambient CO₂ concentration
93 would increase assimilation under full light, but the benefit would be reversed at low light intensity
94 (*PPFD*). For C₄ photosynthesis, achieving this potential will require an appropriate electron
95 transport chain, allowing adequate metabolite traffic, and enlarging the BS to house the biochemical
96 and light harvesting machinery.

97

98 Material and Methods

99 *Overview of the modelling approach*

100 The modelling scheme is depicted in Figure 1 to highlight key inputs and outputs, This model
101 was newly derived to allow a seamless transition between all photosynthetic types except CAM,
102 and joins together an electron transport submodel, a biochemical submodel, a stoichiometric sub-
103 model (see schematic in Figure S1), and a stomatal submodel. The photosynthetic type is defined by
104 setting the strength of the C₄ cycle (as PEP carboxylation rate ($V_{P(J)}$) in the light-limited model and
105 maximum rate of PEPC, ($V_{P\text{MAX}}$) in the enzyme-limited submodel) together with the location of
106 GDC (χ_{GDC}). The electron transport submodel (Note S1) calculates the flux of ATP and NADPH
107 (J_{ATP} and J_{NADPH}) made available under a given *PPFD*. Here, the limitations of previous modelling
108 approaches using a fixed stoichiometry of the electron transport chain (see *Introduction*) were re-
109 solved by allowing the ratio of ATP/NADPH production to be adjusted through mechanisms that
110 were found to be critical in C₄ plants. These are the regulation of the rate of cyclic electron flow
111 (CEF) through the parameter f_{Cyc} , and inducing the NAD(P)H Dehydrogenase-like (NDH) complex
112 (Ivanov *et al.*, 2005; Friso *et al.*, 2010; Munekage *et al.*, 2010) which is characteristic of C₄, and not
113 used by C₃ plants, operating mainly the PGR5 / PGRL1 pathway (Yamori & Shikanai, 2016) by
114 varying f_{NDH} (the fraction of CEF passing through the NDH complex). The reducing power require-
115 ments of nitrogen reduction are implicitly accounted for here as pseudocyclic electron flow (lumped
116 with the water-water cycle, and adjusted through $f_{\text{pseudocyc}}$), in line with Yin and Struik (2012).

117 The biochemical submodel has different formulations depending on the limitation, sharing com-
118 mon underpinnings (Note S2). There is a formulation for limitation by Rubisco or PEPC carboxy-
119 lating capacity (commonly referred to as enzyme limitation, Note S3) and two formulations for
120 light-limited photosynthesis, derived under limiting ATP (Note S4) or NADPH (Note S5). Equa-
121 tions for triose phosphate limited photosynthesis (Busch *et al.*, 2018) were omitted for simplicity as
122 they are relevant under low O₂ or high CO₂ concentrations, or low temperatures (Busch & Sage,
123 2017), while crops like rice – fertilised and irrigated – generally experience mainly light limitations
124 (Yin & Struik, 2015). Similarly, limitations imposed by the diffusion of metabolites (Retta *et al.*,
125 2016) were neglected for simplicity, justified by a recent study addressing the introduction of a
126 weak C₄ cycle in C₃ photosynthesis using a reaction diffusion model that found that any reduction
127 of *A* due to the effect of diffusion processes was limited (Wang *et al.*, 2017). The ATP and NADH
128 produced during respiration were neglected because they are likely to be consumed by basal metab-
129 olism, while NADH imbalances are likely to be dissipated by mitochondrial alternative oxidases
130 (Buckley & Adams, 2011).

131 Using dummy values (initial values for a converging iteration) for the CO₂ concentration at the
132 M carboxylating sites (C_M) the light-limited submodel calculates two distinct sets of outputs, under
133 NADPH and ATP limitations. Of those, that resulting in the minimum V_C is taken as output of the

134 light-limited model. Similarly, starting from C_M , the enzyme-limited submodel calculates a full set
135 of outputs using the kinetic characteristics of Rubisco and PEPC as inputs.

136 Outputs of light-limited and enzyme-limited submodels are joined using a smoothing function
137 to give a continuous output (Note S6), as well as used to calculate τ , a quantity related to the ATP
138 concentration in the M and the BS that acts as the biochemical driver of stomatal response (Note
139 S7). This was included solely to realistically simulate stomatal conductance in a C_3 to C_4 contin-
140 uum, but we make no claim about whether τ offers a faithful mechanistic description of stomatal
141 behaviour. Hydro-mechanical forcing links guard cell responses to the water status and turgor of
142 the leaf, which relate to soil water status and plant hydraulic conductance. The influence of bio-
143 chemical factors relative to hydro-mechanical forcing is determined by the parameter β , while sto-
144 matal morphology is described by χ_S . The output of the stomatal submodel is stomatal conductance,
145 (g_s) that, together with mesophyll conductance g_M , is used to calculate C_M , which is iterated. Tem-
146 perature dependence is simulated with empirical functions (Note S8). For each combination of in-
147 puts, the locality of Rubisco between BS and M (χ_{Rubisco}) together with the rate of flow through CEF
148 (f_{Cyc}) were fitted to maximise A . This resulted in light reactions generating exactly the ATP and
149 NADPH which was consumed by dark reactions, while the ATP-limited model and the NADPH-
150 limited models converged to output the same level of A . The outputs of these submodels (V_{OBS} ,
151 V_{CBS} , V_{OM} , and V_{CM}) were inputted to a generalised stoichiometric model of assimilation (Bellasio,
152 2017), used to calculate reaction rates, and fluxes across the BS and M interface (Figure S1). Here,
153 three additional inputs partition key processes between the BS and M: f_{PR} , for phosphoglycerate re-
154 duction; f_{CS} , for carbohydrate synthesis; f_{PPDK} , for pyruvate phosphate dikinase (Table 1). Model pa-
155 rameterisation and sensitivity are described in Notes S9 and S10, respectively.

156 *Plants, gas exchange, and fluorometry*

157 Plants of *Oryza sativa* subsp. *indica*, modern, high-yielding variety Takanari (Taylaran *et al.*,
158 2009) were germinated and grown in 1.5 L pots filled with Martins potting mix (80% composted
159 bark, 10% coir, 10% sand, complete fertiliser), in acrylate greenhouses located in Canberra (35°S,
160 149°E) under natural illumination in April – May 2018. Pots were partially submerged for a third of
161 the depth in polypropylene tubs and watered weekly for six weeks. Gas exchange and fluorescence
162 were measured on a fully expanded leaf with a setup similar to Bellasio and Griffiths (2014b).
163 Briefly, a portable gas exchange system (LI6400XT, Li-Cor, Lincoln, USA) was modified to oper-
164 ate at low CO_2 concentrations (see licor.com) and fitted with a 6400-06 PAM2000 adapter, holding
165 a fibre probe in the upper leaf cuvette distant enough to avoid shading. Light was provided by a be-
166 spoke red-blue light source, positioned to illuminate uniformly the leaf. Light intensity was meas-
167 ured through an in-chamber Gallium arsenide photodiode, calibrated using a Li-250 light sensor
168 (Li-Cor). Neoprene gaskets were used on both sides of the cuvette. A mixture of 2 % O_2 was pre-
169 pared by mixing ambient air and N_2 with a bespoke gas mixing unit (kindly assembled by Suan

170 Chin Wong). This mix or ambient air was CO₂-scrubbed with soda lime and humidified to a dew
171 point of 15–17 °C upstream of the inlet to maintain water vapour pressure deficit around 1 kPa. CO₂
172 was added from a cylinder (Isi, Vienna, Austria), using the CO₂ injection unit of the LI6400XT.
173 PSII yield was measured with a Dual PAM-F (Heinz Walz GmbH, Effeltrich, Germany). Pulse in-
174 tensity was adjusted to be between 10,000 and 12,000 μmol m⁻² s⁻¹ thereby exceeding the require-
175 ments of between 6,000 and 8,000 μmol m⁻² s⁻¹, depending on CO₂ and *PPFD* levels, to saturate the
176 fluorescence signal. Mass flow leaks (Boesgaard *et al.*, 2013) were monitored with a gas flow meter
177 as detailed in Bellasio *et al.* (2016b), and sealed with a tiny ridge of atoxic gelatine laid between the
178 gaskets and the leaf. Four photosynthetic response curves were measured at 25 °C on *n*=4 plants as
179 detailed in Bellasio *et al.* (2016b). *A/C_i* curves were measured under a *PPFD* of 1200 μmol m⁻² s⁻¹,
180 light curves were measured under a *C_a* of 420 μmol mol⁻¹. Flow rate was 490 μmol s⁻¹; CO₂ diffu-
181 sion through the gaskets was compensated by lengthening the tubing of the LI6400XT reference
182 gas.

183 **Results**

184 *Gas exchange*

185 The operational conditions of rice plants were characterised by a comprehensive gas exchange
186 experiment, which combined measurements under ambient and low O₂. Primary, diffusion leak-
187 corrected data appear as symbols in Figure 2, PSII yield is shown in Figure S3. Overall, rice dis-
188 played typical C₃ responses. Under high *PPFD* (Figure 2A), *A* was lower under ambient O₂ (closed
189 symbols) than under low O₂ (open symbols) because of photorespiration. The quantum yield for as-
190 simation (the initial slope of the curves), was higher under low O₂ (0.0397±0.0002 and
191 0.0512±0.0023 under ambient and low O₂, respectively). Under low *C_i* (Figure 2B), *A* was higher
192 under low O₂ than under ambient O₂ because of O₂ competitive inhibition of Rubisco. Assimilation
193 saturated at relatively lower *C_i* under low O₂ (open symbols) than under ambient O₂. The stomatal
194 conductance (*g_s*) measured in *A/PPFD* curves (Figure 2C) increased monotonically with *PPFD*
195 showing a saturating response similar to that of the *A/PPFD* curve. Under varying external CO₂
196 concentration (*C_a*), *g_s* decreased non-linearly with slope depending on the O₂ level. Rice had a
197 slightly higher *in vivo* *S_{C/O}* (Table 1) than that found *in vitro* (Hermida-Carrera *et al.*, 2016) perhaps
198 for the tight association between mitochondria and chloroplasts that evolved to maximise pho-
199 torespiratory CO₂ recapture (Sage & Sage, 2009; Hatakeyama & Ueno, 2016). Under a *PPFD* of
200 500 μmol m⁻² s⁻¹, rice operated at a relatively low *V_O/V_C* of circa 0.3 [Figure S4, compare with
201 Bellasio *et al.* (2014)].

202 *Simulating assimilation and stomatal conductance of native C₃ rice*

203 A/C_i and $A/PPFD$ curves responses for rice were simulated in the same conditions used for gas
204 exchange measurements. The model predicted with accuracy $A/PPFD$ (Figure 2A) and A/C_i curves
205 (Figure 2B) measured under ambient O_2 , but overestimated $A/PPFD$ and A/C_i curves under low O_2
206 and high C_a . We attribute this to triose phosphate limitation, and to the feedbacks regulating the
207 electron transport chain through the quenching of $Y(II)$ under low O_2 (Figure S3) which we have ad-
208 dressed in Bellasio (2018) but not considered in this model, for simplicity. The simulated stomatal
209 behaviour captures very well the shape of the stomatal response, in both $A/PPFD$ and A/C_i curves
210 and at both O_2 levels.

211 *Simulating gas exchange of C_2 , C_2+C_4 and C_4 rice*

212 Here, simulations were intended to capture hypothetical best-case scenario, assuming unlimited
213 phenotypic plasticity whereby Rubisco is optimally distributed and electron transport processes fully
214 accommodate CEF and NDH levels. Conditions and fitting routines were the same as used for the C_3
215 simulations. The C_2 shuttle and progressive levels of C_4 activity were introduced in native rice by
216 manipulating the activity of PEPC (through the inputs $V_{P_{MAX}}$ and $V_{P(J)}$), the locality of GDC (ξ_{GDC}),
217 the engagement of the NDH pathway of electron transport (f_{NDH}) and the BS apportioning of light
218 respiration (f_{RLIGHT} , see Table 1 for full details). The levels of the fitted inputs $\chi_{Rubisco}$ and f_{Cyc} are
219 shown in Figure S5. These are relevant for bioengineering as they indicate the required physical dis-
220 tribution of Rubisco, and the necessary adjustments to the electron transport chain. $A/PPFD$ curves
221 (Figure 3A) simulated at a C_a of $400 \mu\text{mol mol}^{-1}$ intersect around a $PPFD$ of $300 \mu\text{mol m}^{-2} \text{s}^{-1}$. Under
222 lower $PPFD$ s $C_2 A$ was the highest and C_4 was the lowest. Under higher $PPFD$ s A increased propor-
223 tionally with the level of CCM engagement and was $\sim 22\%$ higher for C_4 than C_3 at a $PPFD$ of 1500
224 $\mu\text{mol m}^{-2} \text{s}^{-1}$. The analysis of A/C_i curves (Figure 3B) revealed expected differences in predicted gas
225 change characteristics between photosynthetic types, with A at C_a lower than $\sim 550 \mu\text{mol mol}^{-1}$ being
226 progressively higher for plants operating CCMs at increasing engagement. But the operation of a
227 CCM necessarily sacrifices A under higher C_a . There were striking differences in stomatal conduct-
228 ance, which was around 40% less in C_4 than in C_3 under a $PPFD$ of $1500 \mu\text{mol m}^{-2} \text{s}^{-1}$ and a C_a of
229 $400 \mu\text{mol mol}^{-1}$ (Figure 3C), indicating that the same level of A was achieved with lower transpiration
230 and higher water use efficiency, in line with differences between extant C_3 and C_4 species (Bellasio
231 *et al.*, 2018; Quirk *et al.*, 2018) although in the field there is some negative feedback on the effect on
232 WUE because of temperature changes. The same differences were maintained in the simulated A/C_i
233 curves (Figure 3D). Notably these differences in g_s resulted solely from biochemical differences be-
234 tween photosynthetic types (sensed by the quantity τ) while all other parameters were maintained at
235 C_3 levels. The operation of the CCMs resulted in an increase in the CO_2 concentration in the BS
236 (Figure 3E and 3F) and in the consequent reduction of the ratio between Rubisco oxygenation and
237 carboxylation (Figure 3G and 3H). The output fraction of BS Rubisco carboxylation V_{CBS}/V_C , which
238 depends both on C_{BS} and on $\chi_{Rubisco}$, is shown in Figure 3I and 3J. V_{CBS}/V_C was relatively invariant

239 with *PPFD* in all photosynthetic types except C_4 , where it slightly decreased below $500 \mu\text{mol m}^{-2} \text{s}^{-1}$
240 (Figure 3I). In *A/Ci* curves $V_{\text{CBS}}/V_{\text{C}}$ increased at low C_a for C_2 and C_2+C_4 types and decreased at high
241 C_a for the C_4 type. Leakiness (the rate of CO_2 retrodiffusion from the BS relative to PEP carboxylation
242 rate), of relevance for isotopic studies, (Cernusak *et al.*, 2013; Bellasio & Griffiths, 2014b) is plotted
243 in Figure S6. To isolate any effect of CO_2 diffusion through the mesophyll and stomata, these simu-
244 lations were repeated using C_M as input, and are shown in Figure S7.

245 *Assimilatory gain/loss of C_2 , C_2+C_4 and C_4 rice at different temperatures, C_a , and *PPFD**

246 This set of simulations explored gains and losses of operating different types of photosynthesis,
247 as compared to C_3 . Three scenarios were simulated: one of unlimited plasticity of the electron
248 transport chain and two in which some elements of the electron transport chain remain in a C_3 con-
249 figuration. In the best case scenario electron transport processes fully accommodate the ATP de-
250 mand of different types of CCM through the optimisation of the levels of CEF (f_{Cyc}) and by allow-
251 ing expression of the NDH complex in C_2+C_4 and C_4 types ($f_{\text{NDH}} > 0$). Figure 4 shows that operating
252 C_2 was beneficial at all temperatures and *PPFD*s, but gains were generally lower than 10% (Figure
253 4B), as compared to C_3 (Figure 4A). Operating C_2+C_4 was slightly counterproductive below a
254 *PPFD* of $450 \mu\text{mol m}^{-2} \text{s}^{-1}$ and a temperature of 40°C but allowed substantial gains above (Figure
255 4C). The range in which operating C_4 photosynthesis did not confer net benefits was cutting diago-
256 nally below a temperature of 40°C and a *PPFD* of $500 \mu\text{mol m}^{-2} \text{s}^{-1}$ (Figure 4D). The possible gains
257 and losses were much more pronounced for C_4 than for C_2 and C_2+C_4 types. In the operation of the
258 C_4 cycle most of the energy saved by suppressing photorespiration is consumed by the regeneration
259 of PEP; the resulting balance depends on their relative flux, and can be quantified through the quan-
260 tum efficiency of assimilation $Y(\text{CO}_2)$, shown on incident light basis in Figure S8. $Y(\text{CO}_2)$ was very
261 similar for C_3 and C_2 types. C_2+C_4 and C_4 had higher $Y(\text{CO}_2)$ than C_3 at high *PPFD*s, but lower at
262 low *PPFD*s. Overall, $Y(\text{CO}_2)$ was slightly lower than our previous measurements in tobacco and
263 maize (Bellasio *et al.*, 2016b; Bellasio *et al.*, 2016a), which we attribute to slightly lower $Y(\text{II})_{\text{LL}}$
264 and s (Table 1).

265 We then compared CCM types to C_3 assimilation in the temperature and C_a space, under a mod-
266 erate *PPFD* of $700 \mu\text{mol m}^{-2} \text{s}^{-1}$, meant to capture illumination of an ordinary erect leaf of a modern
267 cultivar in the upper level of the canopy, in the same optimistic scenario of variable CEF and en-
268 gaged NDH (Figure 4E). C_2 assimilation was beneficial at all temperatures and C_a (Figure 4F).
269 Gains were greater than 10% in a relatively broad set of conditions including under ambient C_a at
270 high temperatures. The C_4 and C_2+C_4 types were disadvantageous above a C_a of around 450
271 $\mu\text{mol mol}^{-1}$ and below 40°C – a broader range than under higher *PPFD* (Figure 3B). The C_4 and
272 C_2+C_4 types were progressively more advantageous at higher temperature and low C_a .

273 Similar simulations were carried out to represent a less optimistic scenario whereby the activity
274 of the NDH complex remained at C_3 levels ($f_{\text{NDH}} = 0$) for all photosynthetic types (Figure 5, top

275 row). The marginal gains were maintained for the C₂ type (Figure 5A); however, C₂+C₄ and C₄
276 types were counterproductive in a broader range of *PPFD*s roughly cutting below a *PPFD* of 700
277 $\mu\text{mol m}^{-2} \text{s}^{-1}$ for the C₂+C₄ type and 900 $\mu\text{mol m}^{-2} \text{s}^{-1}$ for the C₄ type (Figure 5B and 5C).

278 In a pessimistic scenario, in addition to the incapacity to express sufficient NDH complex
279 ($f_{\text{NDH}}=0$), CCM types were unable to modify the flux through CEF, which remained capped at C₃
280 levels (Figure 5, bottom row). Here, the marginal gains were maintained for C₂ photosynthesis (Fig-
281 ure 5D); however, the C₂+C₄ type was counterproductive below a *PPFD* of 1000 $\mu\text{mol m}^{-2} \text{s}^{-1}$,
282 while the C₄ type was counterproductive at all *PPFD*s below a temperature of 30°C (Figure 5E and
283 5F). Severe losses in excess of 40% were predicted for the C₄ type at ordinary temperatures and
284 moderate to low *PPFD*s.

285 *Metabolite transport*

286 Two further sets of simulations estimated the metabolite fluxes between the M and the BS by
287 manipulating the level of C₄ engagement through increasing levels of V_P (Figure 6) so as to repre-
288 sent the full C₂+C₄ continuum from C₂ (left of each panel) to C₄ (right of each panel). In a first sce-
289 nario (Figure 6A), the level of ATP demand in the BS was minimised. In these conditions, phospho-
290 glycerate is not reduced in the BS but diffuses to the M and is reduced therein to dihydroxyacetone
291 phosphate, DHAP. A minimal part of DHAP is used by carbohydrate synthesis, but the majority dif-
292 fuses back to BS to replenish the sugar phosphates pool. This drives the metabolite exchange be-
293 tween the M and the BS to a maximum. In addition, because phosphoglycerate reduction is the main
294 NADPH sink in the BS, when ATP demand in the BS is minimal, the NADPH demand in the BS is
295 also minimal. This requires by-passing the malate dehydrogenase in the M, and, to maintain the ef-
296 ficiency of the CCM despite the inability to operate the malate shuttle, the CCM works through ala-
297 nine and aspartate (Bellasio, 2017). This condition is suboptimal because it requires high concentra-
298 tion gradients of aspartate and alanine when malate and pyruvate do not transport CO₂ (Arrivault *et*
299 *al.*, 2017). At low levels of C₄ engagement, when V_P was low, glycine and serine were operating the
300 C₂ shuttle. The model predicts that the reducing power generated in the BS by the decarboxylation
301 of glycine, which could not be used by phosphoglycerate reduction because of the insufficient ATP
302 availability, was returned to the M by the malate and pyruvate shuttle in a ‘backward’ C₄ cycle. As
303 V_P increased, the flux of glycine and strength of the C₂ cycle [which scales with V_P , see details in
304 Bellasio (2017)] was progressively reduced, diminishing the excess NADPH in BS together with
305 the malate and pyruvate fluxes that decrease to zero with V_P . With the increase in V_P , the fitted frac-
306 tion of Rubisco carboxylation in BS increased linearly, causing the ratio of ATP demand in BS rela-
307 tive to M to increase linearly (Figure 6C).

308 An opposite scenario, where fluxes were minimal, was simulated by fitting f_{PR} and f_{CS} to mini-
309 mize the sum of squared flow rates between BS and M (Figure 6B). In these conditions the increase
310 of phosphoglycerate reduction in the BS drove the ATP demand in the BS to a maximum (Figure

311 6D). The total fluxes were less than half those of the previous case (54 *versus* 130 $\mu\text{mol m}^{-2} \text{s}^{-1}$); the
312 main metabolites to be transported in these conditions were malate and pyruvate, which were the
313 sole compounds to support the CCM while the flux of aminoacids was minimal. Despite the malate
314 and pyruvate shuttle working in full, and exporting reducing power from the M to the BS, the
315 NADPH demand in the BS was high (Figure 6D), requiring substantial linear electron flow in the
316 BS ($\sim 18 \mu\text{mol m}^{-2} \text{s}^{-1}$ of NADPH).

317 **Discussion**

318 This work set out to study the theoretical underpinnings of the introduction of CCMs into C_3 me-
319 tabolism. A model of enzyme and light-limited assimilation was newly derived to account for the
320 stoichiometry of Bellasio (2017), augmented to include the explicit mechanistic description of the
321 electron transport chain (Bellasio, 2018), and a hydromechanical and biochemical model of sto-
322 matal conductance recently shown to work for C_3 and C_4 plants (Bellasio *et al.*, 2017). We shall
323 stress four points distinguishing the importance of this work. Firstly, by including a hydromechani-
324 cal submodel we provide a means to connect plant assimilatory biochemistry to plant hydraulics,
325 allowing the concurrent investigation of photosynthesis and water use. Secondly, this is the only
326 study comparing C_2 performance with C_3 , C_2+C_4 and C_4 seamlessly within a single model, offering
327 a further improvement over approaches targeted to specific types. Thirdly, this is the only study es-
328 timating the metabolite fluxes necessary to operate the different photosynthetic types. Lastly, the
329 model marries biochemically comprehensiveness (it includes all main reactions of the photosyn-
330 thetic metabolism) with computational speed, required by larger scale modelling. This model is
331 generally applicable, and will be valuable for ecophysiological and evolutionary studies, but we will
332 address evolution at a later stage. Here, we applied the modelling framework to predict assimilation
333 and metabolite fluxes in a three dimensional environmental landscape ($t \times C_a \times PPF$) using pa-
334 rameters derived for rice. Next, we make some general considerations on the introduction of a CCM
335 in C_3 metabolism, and we elaborate on the special case of rice.

336 There is a pervasive belief that the introduction of C_4 photosynthesis into C_3 plants will uncondi-
337 tionally increase assimilation, supported by models based on the assumption that ATP and NADPH
338 are unlimited (Heckmann *et al.*, 2013). However, decades of comparison between C_4 and C_3 plants
339 have shown that C_3 plants may be advantaged in a range of conditions [e.g. (Ehleringer *et al.*, 1997;
340 Ghannoum *et al.*, 2000; Christin & Osborne, 2014)]. We showed that, when energy budgets were
341 accounted for, C_4 photosynthesis becomes unfavourable at high CO_2 concentrations, low $PPFD$ and
342 low temperatures, and therefore provide a novel theoretical framework to explain such experimental
343 observations.

344 *Bundle sheath permeability mediates trade-offs imposed by light intensity*

345 Modern crops like rice have typically a LAI (leaf area per ground area) of 5–6, meaning that the
346 majority of leaves are shaded and, importantly, the overall performance of C₄ types will compro-
347 mise full–light advantages and shade disadvantages. The key parameter governing photosynthetic
348 losses under low *PPFD* in C₄ photosynthesis is BS conductance, g_{BS} (Bellasio & Griffiths, 2014b).
349 g_{BS} controls the flux of CO₂ released in the BS that retrodiffuses to the M, called leakage (Farquhar,
350 1983). g_{BS} can vary several orders of magnitude in nature and can affect *A* substantially (Kromdijk
351 *et al.*, 2014; Yin & Struik, 2017), in particular at high levels of CCM engagement (Figure S9). Un-
352 der high temperature, g_{BS} is reported to increase (Yin *et al.*, 2016), while under low *PPFD* V_P de-
353 creases, driven by a reduced rate of ATP production (Bellasio & Griffiths, 2014b). In these condi-
354 tions, leakage reduces C_{BS} , and, in C₄ plants, it dissipates energy through the ATP–dependent re-
355 generation of phosphoenolpyruvate required to re–fix the leaked CO₂, making the CCM counterpro-
356 ductive (Tazoe *et al.*, 2008; Ubierna *et al.*, 2011; Ubierna *et al.*, 2013; Bellasio & Griffiths, 2014b;
357 Sun *et al.*, 2014; Pignon *et al.*, 2017). In nature, plants minimise the ratio between leakage and me-
358 tabolite fluxes by preferentially localising plasmodesmata at the interface between M and BS, while
359 apoplastic diffusion is often reduced by the deposition of a gas–tight suberized cell wall (Sowinski
360 *et al.*, 2008; Sowiński, 2013; Danila *et al.*, 2016; Danila *et al.*, 2018). If low g_{BS} may therefore ap-
361 pear desirable (though perhaps difficult to achieve), high symplastic permeability is required to sus-
362 tain metabolite diffusion [Figure 6, (Weber & von Caemmerer, 2010)], and this dilemma constitutes
363 an efficiency trade–off that is inherent to the C₄ CCM – and unavoidable (Bellasio & Griffiths,
364 2014a). Indeed, to attune leakage to *PPFD* levels, g_{BS} in maize was found to adjust during growth
365 (Bellasio & Griffiths, 2014b) as well as in adult leaves (Bellasio & Griffiths, 2014a).

366 *Future CO₂ levels*

367 Rising anthropogenic atmospheric CO₂ concentrations will favour C₃ assimilation over C₄. Apart
368 from the difficulties in predicting future CO₂ levels – not addressed here – predicting assimilation
369 under changing CO₂ is very difficult. When plants are exposed to a high CO₂ level for a long time
370 they may downregulate the pool of Rubisco and PEPC (Ghannoum *et al.*, 2000; Leakey *et al.*, 2004;
371 Long *et al.*, 2006; Leakey *et al.*, 2012), at the same time, producing fewer stomata (Way *et al.*,
372 2011; Franks *et al.*, 2012)(Quirk, Bellasio and Beerling, *Annals of Botany*, *in press.*). There is a
373 growing body of data gained under controlled conditions [e.g. (Bellasio *et al.*, 2018; Quirk *et al.*,
374 2018)] and in free air experiments [e.g. (Bishop *et al.*, 2015)], yet, responses are species specific
375 and, currently, evidence is not sufficient to generalise acclimation responses of C₄ and C₃ plants. As
376 a result, it is common practice in climate modelling to take assimilatory responses measured under
377 transient changes in CO₂ levels (*A/C_a* curves) as predictive of stable responses of plants grown un-
378 der different CO₂ levels, that is, no large scale models include representation of the physiological
379 acclimation to future CO₂ level (Rogers *et al.*, 2017). With this principle, using simple interpolation
380 of the best case scenario shown in Figure 4H, at 25 °C, C₄ assimilation would equal C₃ assimilation

381 at a C_a of $465 \mu\text{mol mol}^{-1}$, a level that would be exceeded in 2036 according to the A2 scenario of
382 carbon emission mitigation (http://www.ipcc-data.org/observ/ddc_co2.html).

383 *Strategies for engineering a CCM*

384 In the face of global warming, the introduction of CCMs in a C_3 crop such as rice was proposed
385 as a possible strategy to increase yield (Leegood, 2013; Long *et al.*, 2015). An operational C_2 shut-
386 tle was considered as a first step in bio-engineering, with the final goal of obtaining a fully ex-
387 pressed C_4 type. Of the three biochemical C_4 subtypes (NADP-ME, NAD-ME, PEPCK), the
388 NADP-ME was chosen as the initial target (Kajala *et al.*, 2011), as it is operated by the crops with
389 greatest productivity (Furbank, 2011) and would require introducing a smaller number of enzymes
390 [in M cells carbonic anhydrase, PEPC, malate dehydrogenase, and pyruvate-phosphate dikinase; in
391 BS cells NADP-ME, plus eight transmembrane transporters (Kajala *et al.*, 2011)]. Other subtypes
392 require additional enzymes [aspartate and alanine aminotransferase, PEPCK, NAD-ME (Wang *et*
393 *al.*, 2014), plus up to three transporters (Schlüter *et al.*)] and were not considered here, but see
394 Bellasio (2017). Traditionally, strategies for engineering a CCM have emphasized the manipulation
395 of dark reactions and the associated genetics (Kajala *et al.*, 2011; Leegood, 2013). Here we point to
396 two overlooked factors required for the operation of a CCM, namely anatomy and light reactions.

397 Firstly, leaf anatomy needs to be adjusted depending on the level of C_4 cycle expression. Anat-
398 omy and biochemistry of the BS are mutually interdependent (Bellasio & Griffiths, 2014c). The re-
399 quirement in light harvesting optical cross section depends on the ATP demand, and determines the
400 required BS volume, mediated by the size of the ATP-generating light harvesting machinery, plus
401 the volume of the dark reactions machinery (Bellasio & Lundgren, 2016). Minimal ATP demand in
402 the BS may be desirable as it would require the smallest BS, and therefore require minimum modi-
403 fication of the current rice anatomy, but would lead to the unwanted necessity of high gradients and
404 flux rates, and require the expression of high levels of metabolite transporters (Pick *et al.*, 2011).
405 Aiming at a high ATP demand would have the benefit of requiring the minimum expression of
406 transporters but would require the largest electron transport chain, and therefore a more radical
407 modification of the native C_3 anatomy. Identifying a desired anatomical target requires therefore
408 first to identify a biochemical ideotype. Each of the two extreme solutions shown in Figure 6 would
409 entail limited operational robustness (Pick *et al.*, 2011), as there would not be any freedom to ac-
410 commodate transient environmental change (Bellasio & Griffiths, 2014c). A ‘robust flexibility’
411 would be positioned half-way between these two opposite scenarios, for instance where the ATP
412 demand in the BS relative to M is 0.7. The potential ratio of ATP production in the BS relative to M
413 must exceed 0.7 by a considerable safety margin (Bellasio & Lundgren, 2016) to counter changing
414 light conditions (Bellasio & Griffiths, 2014c). To achieve this, the light absorbed in the BS relative
415 to M under white light, must be close to 0.7. Currently, the size and pigmentation of rice BS is in-
416 sufficient (Bellasio & Lundgren, 2016). A suitable situation was found in maize, which had a BS

417 pigmentation circa twice that of the M, and allocated ~30% of the total leaf section area to the BS
418 (Bellasio & Lundgren, 2016) and should be considered as the target for C₄ rice. Further, reaching
419 the required levels for g_{BS} will require engineering the appropriate density of plasmodesmata
420 (Danila *et al.*, 2016), reducing leakage, and possibly allow for acclimation of g_{BS} during growth
421 (see above). Alternatively, higher efficiency could be reached by operating the C₄ cycle only in
422 those parts of the canopy where the *PPFD* is higher than a given threshold, but this seems difficult
423 to achieve also because it is adopted neither in mature nor in developing maize leaves (Wang *et al.*,
424 2013).

425 Secondly, the operation of a C₄ cycle will require important modifications to the electron
426 transport chains. We showed that when cyclic electron flow, CEF (f_{Cyc}) and the NDH pathway
427 (f_{NDH}) were allowed to vary (Figure 4), the performance of C₂+C₄ and C₄ types was maximal. This
428 optimal scenario reflects the idea that electron transport processes may spontaneously adjust in re-
429 sponse to the expression of a CCM, responding to an increase in ATP demand, through flexibility
430 mechanisms inherent in native chloroplasts (Takeuchi *et al.*, 2000). Higher levels of f_{NDH} would
431 benefit C₄ assimilation, but may be physiologically implausible, for example because NDH is very
432 expensive to produce and maintain. It is possible, however, that rice does not have the potential to
433 express adequate level of CEF and NDH components. If f_{NDH} is capped at C₃ levels the performance
434 of C₄ rice will be lower (Figure 5 A–C), and if f_{Cyc} is capped at C₃ levels *A* would be depressed even
435 further (Figure 5 D–F).

436 Considering the complexities and trade-offs of implementing a C₄ cycle, C₂ rice may be a desir-
437 able product of bioengineering efforts. Despite the relative operational simplicity, the engagement
438 of a C₂ shuttle always increased assimilation rate, relative to C₃. The assimilation gain was rela-
439 tively small under ambient C_a , but increased with temperature at low C_a (Figure 4F). Although in
440 water-rich rice paddies plants can maintain stomata open and extreme photorespiratory conditions
441 might not occur at mid-latitudes (where temperatures are milder and the subsp. *japonica* is fa-
442 voured), they may occur at low-latitudes (where temperatures are higher and the subsp. *indica* is
443 favoured), and, particularly, for dryland rice, which would probably be the crop to benefit most
444 from the introduction of a C₂ CCM. In the simulations, the locality of Rubisco activity, as $\chi_{Rubisco}$,
445 was adjusted continuously at varying C_M always resulting in optimal Rubisco activity. In nature,
446 however, the proportion of Rubisco in the BS may change only on evolutionary timescales and may
447 be plant-specific. Consequently, there may be a trade-off between optimisation for photorespira-
448 tory conditions, by compartmentalising more Rubisco to the BS, or for non-photorespiratory condi-
449 tions by allowing all Rubisco in the M, with easier access to intercellular CO₂. Allocating 10 % of
450 Rubisco in the BS was a good compromise (Figure S5).

451 *From leaf-level to crop*

452 Upscaling these findings to calculate crop yield will be a challenging task. Firstly, it will require
453 modelling of the canopy light environment (Song *et al.*, 2013), possibly including diel light cycles
454 of fully illuminated leaves (Wu *et al.*, 2017) and the transient illumination in shaded leaves (Pearcy
455 *et al.*, 1997), nitrogen allocation (Buckley *et al.*, 2002; Dewar *et al.*, 2012), the effect of different
456 canopy architectures (Burgess *et al.*, 2017), the response of A and g_s to temperature and humidity
457 (Yin & Struik, 2017). Ideally, the description could consider the potential losses due to suboptimal
458 stomatal aperture (Violet-Chabrand *et al.*, 2016; Bellasio *et al.*, 2017), and the mid-morning depres-
459 sions of photosynthetic capacity (Horton & Murchie, 2000). The necessity of translating assimila-
460 tion into grain yield will add further complexities and require a dedicated crop model accounting for
461 root growth, nitrogen uptake, pathogens, as well as the interactions between cultivars and climate
462 (Li *et al.*, 2015; Paleari *et al.*, 2017). There is an urgent need for addressing some of these chal-
463 lenges. This model offers the necessary underpinnings and can be readily used as a submodel for
464 modelling assimilation at higher spatial level.

465 **Conclusion**

466 We developed new ATP-limited, and NADPH-limited submodels of assimilation, as well as a
467 light reaction submodel, coupled with a stomatal submodel. The resulting model connects light har-
468 vesting to dark assimilatory biochemistry and hydraulics and is valid for any photosynthetic type.
469 The equations were solved analytically and will be valuable for evolutionary as well as ecophysio-
470 logical studies, and we encourage their use also for larger scale modelling. The model was cali-
471 brated and tested on primary gas exchange and fluorescence data measured on rice. By simulating
472 the introduction of CCMs in C_3 metabolism we showed that C_4 photosynthesis becomes disadvanta-
473 geous under a set of environmental conditions (low light, low temperatures and high CO_2) thus
474 providing theoretical support for decades of ecophysiological observations. For the expression of a
475 CCM to be advantageous, any modifications to dark reactions need to be accompanied by substan-
476 tial modifications to light reactions. Specifically, engineering an appropriate electron transport
477 chain, with the possibility of expressing the NDH complex and adjusting levels of cyclic electron
478 flow will be required. These will also need to be accompanied by anatomical modifications to ac-
479 commodate the biochemical and light harvesting machinery and by the expression of suitable levels
480 of transporters to allow adequate metabolite traffic.

481 **Acknowledgments**

482 We are grateful to Ross Deans, Joe Quirk, Florian Busch, and Pascal-Antoine Christin for re-
483 view, to Alexis Moschopoulos, Emily Beardon, Yuzhen Fan, and Deyun Qiu for plants, to Rosario
484 Maggistro for help, to Dean Price for the fluorometer, to Susanne von Caemmerer and Suan Chin
485 Wong for gas exchange equipment, to Tom Sharkey for initially suggesting to apply the model to

486 the introduction of the C₄ cycle in rice. CB gratefully acknowledges funding through a H2020 Ma-
487 rie Skłodowska–Curie individual fellowship (DILIPHO, ID: 702755). GDF gratefully acknowl-
488 edges the ARC Centre of Excellence for Translational Photosynthesis (Grant number
489 CE140100015).

490 This work was solely driven by the Authors' curiosity, is not part of – and is not funded by –
491 projects aimed at creating C₄ rice; the Authors have no conflict of interest.

492 **Author Contributions**

493 CB conceived of the research, performed measurements, developed and coded the models, ran
494 simulations. CB and GDF wrote the paper.

495 **Availability**

496 The model, coded in Excel, is made freely available in Supporting Information. The model does
497 not include 'live' scripts and is fully operational in the open access suite 'Apache Open Office'.

References

- Arrivault S, Obata T, Szc wka M, Mengin V, Guenther M, Hoehne M, Fernie AR, Stitt M. 2017. Metabolite pools and carbon flow during C₄ photosynthesis in maize: ¹³CO₂ labeling kinetics and cell type fractionation. *Journal of Experimental Botany* **68**(2): 283-298.
- Atkinson RRL, Mockford EJ, Bennett C, Christin P-A, Spriggs EL, Freckleton RP, Thompson K, Rees M, Osborne CP. 2016. C₄ photosynthesis boosts growth by altering physiology, allocation and size. *Nature Plants* **2**: 16038.
- Bellasio C. 2017. A generalised stoichiometric model of C₃, C₂, C₂+C₄, and C₄ photosynthetic metabolism. *Journal of Experimental Botany* **68**(2): 269-282.
- Bellasio C. 2018. A generalised dynamic model of leaf-level C₃ photosynthesis combining light and dark reactions with stomatal behaviour. *Photosynthesis Research* **10.1007/s1120-018-0601-1**.
- Bellasio C, Beerling DJ, Griffiths H. 2016a. Deriving C₄ photosynthetic parameters from combined gas exchange and chlorophyll fluorescence using an Excel tool: theory and practice. *Plant, Cell & Environment* **39**(6): 1164-1179.
- Bellasio C, Beerling DJ, Griffiths H. 2016b. An Excel tool for deriving key photosynthetic parameters from combined gas exchange and chlorophyll fluorescence: theory and practice. *Plant Cell and Environment* **39**(6): 1180-1197.
- Bellasio C, Burgess SJ, Griffiths H, Hibberd JM. 2014. A high throughput gas exchange screen for determining rates of photorespiration or regulation of C₄ activity. *Journal of Experimental Botany* **65**(13): 3769-3779.
- Bellasio C, Griffiths H. 2014a. Acclimation of C₄ metabolism to low light in mature maize leaves could limit energetic losses during progressive shading in a crop canopy. *Journal of Experimental Botany* **65**(13): 3725-3736.
- Bellasio C, Griffiths H. 2014b. Acclimation to Low Light by C₄ maize: Implications for Bundle Sheath Leakiness. *Plant Cell and Environment* **37**(5): 1046-1058.
- Bellasio C, Griffiths H. 2014c. The operation of two decarboxylases (NADPME and PEPCK), transamination and partitioning of C₄ metabolic processes between mesophyll and bundle sheath cells allows light capture to be balanced for the maize C₄ pathway. *Plant Physiology* **164**: 466-480.
- Bellasio C, Lundgren MR. 2016. Anatomical constraints to C₄ evolution: light harvesting capacity in the bundle sheath. *New Phytologist* **212**(2): 485-496.
- Bellasio C, Quirk J, Beerling DJ. 2018. Stomatal and non-stomatal limitations in savanna trees and C₄ grasses grown at low, ambient and high atmospheric CO₂. *Plant Science* **274**: 181-192.
- Bellasio C, Quirk J, Buckley TN, Beerling D. 2017. A dynamic hydro-mechanical and biochemical model of stomatal conductance for C₄ photosynthesis. *Plant Physiology* **175**: 104-119.
- Bishop KA, Betzelberger AM, Long SP, Ainsworth EA. 2015. Is there potential to adapt soybean (*Glycine max* Merr.) to future [CO₂]? An analysis of the yield response of 18 genotypes in free-air CO₂ enrichment. *Plant, Cell & Environment* **38**(9): 1765-1774.
- Boesgaard KS, Mikkelsen TN, Ro-Poulsen H, Ibrom A. 2013. Reduction of molecular gas diffusion through gaskets in leaf gas exchange cuvettes by leaf-mediated pores. *Plant, Cell & Environment* **36**(7): 1352-1362.
- Buckley TN, Adams MA. 2011. An analytical model of non-photorespiratory CO₂ release in the light and dark in leaves of C₃ species based on stoichiometric flux balance. *Plant, Cell & Environment* **34**(1): 89-112.
- Buckley TN, Miller JM, Farquhar GD. 2002. The mathematics of linked optimisation for water and nitrogen use in a canopy. *Silva Fennica* **36**(3): 639-669.
- Buckley TN, Sack L, Farquhar GD. 2016. Optimal plant water economy. *Plant, Cell & Environment* **40**(6): 881-896.
- Burgess AJ, Retkute R, Herman T, Murchie EH. 2017. Exploring Relationships between Canopy Architecture, Light Distribution, and Photosynthesis in Contrasting Rice Genotypes Using 3D Canopy Reconstruction. *Frontiers in Plant Science* **8**: 734.
- Busch FA, Sage RF. 2017. The sensitivity of photosynthesis to O₂ and CO₂ concentration identifies strong Rubisco control above the thermal optimum. *New Phytologist* **213**(3): 1036-1051.
- Busch FA, Sage RF, Farquhar GD. 2018. Plants increase CO₂ uptake by assimilating nitrogen via the photorespiratory pathway. *Nature Plants* **4**: 46-54.
- Cernusak LA, Ubierna N, Winter K, Holtum JAM, Marshall JD, Farquhar GD. 2013. Environmental and physiological determinants of carbon isotope discrimination in terrestrial plants. *New Phytologist* **200**: 950-965.
- Christin PA, Osborne CP. 2014. The evolutionary ecology of C₄ plants. *New Phytologist* **204**(4): 765-781.
- Covshoff S, Szc wka M, Hughes TE, Smith-Unna R, Kelly S, Bailey KJ, Sage TL, Pachebat JA, Leegood R, Hibberd JM. 2016. C₄ Photosynthesis in the Rice Paddy: Insights from the Noxious Weed *Echinochloa glabrescens*. *Plant Physiology* **170**(1): 57-73.
- Danila F, Quick WP, White RG, Furbank RT, von Caemmerer S. 2016. The Metabolite Pathway between Bundle Sheath and Mesophyll: Quantification of Plasmodesmata in Leaves of C₃ and C₄ Monocots. *The Plant Cell* **28**(6): 1461-1471.
- Danila FR, Quick WP, White RG, Kelly S, von Caemmerer S, Furbank RT. 2018. Multiple mechanisms for enhanced plasmodesmata density in disparate subtypes of C₄ grasses. *Journal of Experimental Botany* **69**(5): 1135-1145.
- Dewar RC, Tarvainen L, Parker K, Wallin G, McMurtrie RE. 2012. Why does leaf nitrogen decline within tree canopies less rapidly than light? An explanation from optimization subject to a lower bound on leaf mass per area. *Tree Physiology* **32**(5): 520-534.
- Ehleringer JR, Cerling TE, Helliker BR. 1997. C₄ photosynthesis, atmospheric CO₂, and climate. *Oecologia* **112**(3): 285-299.
- Evans JR, von Caemmerer S, Vogelmann TC. 2007. Balancing light capture with distributed metabolic demand during C₄ photosynthesis. In: J.E. S, P.L. M, B. H eds. *Charting new pathways to C₄ rice*: IRRI International Rice Research Institute.
- Farquhar G, Wong S. 1984. An empirical model of stomatal conductance. *Functional Plant Biology* **11**(3): 191-210.
- Farquhar GD. 1983. On the Nature of Carbon Isotope Discrimination in C₄ Species. *Australian Journal of Plant Physiology* **10**(2): 205-226.

- Franks PJ, Leitch IJ, Ruzsala EM, Hetherington AM, Beerling DJ. 2012. Physiological framework for adaptation of stomata to CO₂ from glacial to future concentrations. *Philosophical Transactions of the Royal Society B-Biological Sciences* **367**(1588): 537-546.
- Friso G, Majeran W, Huang MS, Sun Q, van Wijk KJ. 2010. Reconstruction of Metabolic Pathways, Protein Expression, and Homeostasis Machineries across Maize Bundle Sheath and Mesophyll Chloroplasts: Large-Scale Quantitative Proteomics Using the First Maize Genome Assembly. *Plant Physiology* **152**(3): 1219-1250.
- Furbank RT. 2011. Evolution of the C₄ photosynthetic mechanism: are there really three C₄ acid decarboxylation types? *Journal of Experimental Botany* **62**(9): 3103-3108.
- Galmés J, Hermida-Carrera C, Laanisto L, Niinemets Ü. 2016. A compendium of temperature responses of Rubisco kinetic traits: variability among and within photosynthetic groups and impacts on photosynthesis modeling. *Journal of Experimental Botany* **67**(17): 5067-5091.
- Ghannoum O, Caemmerer SV, Ziska LH, Conroy JP. 2000. The growth response of C₄ plants to rising atmospheric CO₂ partial pressure: a reassessment. *Plant, Cell & Environment* **23**(9): 931-942.
- Gowik U, Bräutigam A, Weber KL, Weber APM, Westhoff P. 2011. Evolution of C₄ Photosynthesis in the Genus *Flaveria*: How Many and Which Genes Does It Take to Make C₄? *The Plant Cell Online* **23**(6): 2087-2105.
- Hahn A, Vonck J, Mills DJ, Meier T, Kühlbrandt W. 2018. Structure, mechanism, and regulation of the chloroplast ATP synthase. *Science* **360**(6389): eaat4318.
- Hatakeyama Y, Ueno O. 2016. Intracellular position of mitochondria and chloroplasts in bundle sheath and mesophyll cells of C₃ grasses in relation to photorespiratory CO₂ loss. *Plant Production Science* **19**(4): 540-551.
- Heckmann D, Schulze S, Denton A, Gowik U, Westhoff P, Weber Andreas PM, Lercher Martin J. 2013. Predicting C₄ Photosynthesis Evolution: Modular, Individually Adaptive Steps on a Mount Fuji Fitness Landscape. *Cell* **153**(7): 1579-1588.
- Hermida-Carrera C, Kapralov MV, Galmés J. 2016. Rubisco catalytic properties and temperature response in crops. *Plant Physiology*: pp. 01846.02016.
- Horton P, Murchie EH 2000. C₄ photosynthesis in rice: some lessons from studies of C₃ photosynthesis in field-grown rice*. In: J.E. Sheehy PLM, Hardy B eds. *Studies in Plant Science*: Elsevier, 127-144.
- Ishikawa N, Takabayashi A, Sato F, Endo T. 2016. Accumulation of the components of cyclic electron flow around photosystem I in C₄ plants, with respect to the requirements for ATP. *Photosynthesis Research*: 1-17.
- Ivanov B, Asada K, Kramer DM, Edwards G. 2005. Characterization of photosynthetic electron transport in bundle sheath cells of maize. I. Ascorbate effectively stimulates cyclic electron flow around PSI. *Planta* **220**(4): 572-581.
- Jurić I, González-Pérez V, Hibberd JM, Edwards G, Burroughs NJ. 2017. Size matters for single-cell C₄ photosynthesis in *Bienertia*. *Journal of Experimental Botany* **68**(2): 255-267.
- Kajala K, Covshoff S, Karki S, Woodfield H, Tolley BJ, Dionora MJA, Mogul RT, Mabilangan AE, Danila FR, Hibberd JM, et al. 2011. Strategies for engineering a two-celled C₄ photosynthetic pathway into rice. *Journal of Experimental Botany* **62**(9): 3001-3010.
- Kanai R, Edwards GE 1999. The biochemistry of C₄ photosynthesis. In: Sage RF, Monson RK eds. *C₄ plant biology*. San Diego: Academic Press.
- Keerberg O, Pärnik T, Ivanova H, Bassüner B, Bauwe H. 2014. C₂ photosynthesis generates about 3-fold elevated leaf CO₂ levels in the C₃-C₄ intermediate species *Flaveria pubescens*. *Journal of Experimental Botany* **65**(13): 3649-3656.
- King JL, Edwards GE, Cousins AB. 2012. The efficiency of the CO₂-concentrating mechanism during single-cell C₄ photosynthesis. *Plant, Cell & Environment* **35**(3): 513-523.
- Kromdijk J, Ubierna N, Cousins AB, Griffiths H. 2014. Bundle-sheath leakiness in C₄ photosynthesis: a careful balancing act between CO₂ concentration and assimilation. *Journal of Experimental Botany* **65**(13): 3443-3457.
- Leakey ADB, Ainsworth EA, Bernacchi CJ, Zhu X, Long SP, Ort DR 2012. Photosynthesis in a CO₂-Rich Atmosphere. In: Eaton-Rye JJ, Tripathy BC, Sharkey TD eds. *Photosynthesis: Plastid Biology, Energy Conversion and Carbon Assimilation*. Dordrecht: Springer Netherlands, 733-768.
- Leakey ADB, Bernacchi CJ, Dohleman FG, Ort DR, Long SP. 2004. Will photosynthesis of maize (*Zea mays*) in the US Corn Belt increase in future [CO₂] rich atmospheres? An analysis of diurnal courses of CO₂ uptake under free-air concentration enrichment (FACE). *Global Change Biology* **10**(6): 951-962.
- Leegood RC. 2013. Strategies for engineering C₄ photosynthesis. *Journal of Plant Physiology* **170**(4): 378-388.
- Li T, Hasegawa T, Yin X, Zhu Y, Boote K, Adam M, Bregaglio S, Buis S, Confalonieri R, Fumoto T. 2015. Uncertainties in predicting rice yield by current crop models under a wide range of climatic conditions. *Global Change Biology* **21**(3): 1328-1341.
- Long SP, Ainsworth EA, Leakey ADB, Nösberger J, Ort DR. 2006. Food for thought: Lower-than-expected crop yield stimulation with rising CO₂ concentrations. *Science* **312**(5782): 1918-1921.
- Long S P, Marshall-Colon A, Zhu X-G. 2015. Meeting the Global Food Demand of the Future by Engineering Crop Photosynthesis and Yield Potential. *Cell* **161**(1): 56-66.
- Lundgren MR, Osborne CP, Christin P-A. 2014. Deconstructing Kranz anatomy to understand C₄ evolution. *Journal of Experimental Botany* **65**(13): 3357-3369.
- Meyer M, Griffiths H. 2013. Origins and diversity of eukaryotic CO₂-concentrating mechanisms: lessons for the future. *Journal of Experimental Botany* **64**(3): 769-786.
- Monson RK, Moore Bd. 1989. On the significance of C₃-C₄ intermediate photosynthesis to the evolution of C₄ photosynthesis. *Plant, Cell & Environment* **12**(7): 689-699.
- Monteith JL. 1978. Reassessment of Maximum Growth-Rates for C₃ and C₄ Crops. *Experimental Agriculture* **14**(1): 1-5.
- Munekage YN, Eymery F, Rumeau D, Cuine S, Oguri M, Nakamura N, Yokota A, Genty B, Peltier G. 2010. Elevated Expression of PGR5 and NDH-H in Bundle Sheath Chloroplasts in C-4 *Flaveria* Species. *Plant and Cell Physiology* **51**(4): 664-668.

- Osmond C, Smith F 1976.** Symplastic transport of metabolites during C₄-photosynthesis. *Intercellular communication in plants: Studies on plasmodesmata*: Springer, 229-241.
- Paleari L, Movedi E, Cappelli G, Wilson LT, Confalonieri R. 2017.** Surfing parameter hyperspaces under climate change scenarios to design future rice ideotypes. *Global Change Biology*.
- Pearcy RW, Ehleringer J. 1984.** Comparative ecophysiology of C₃ and C₄ plants. *Plant, Cell & Environment* **7**(1): 1-13.
- Pearcy RW, Gross LJ, He D. 1997.** An improved dynamic model of photosynthesis for estimation of carbon gain in sunflecks light regimes. *Plant Cell and Environment* **20**(4): 411-424.
- Pick TR, Brautigam A, Schlüter U, Denton AK, Colmsee C, Scholz U, Fahnenstich H, Pieruschka R, Rascher U, Sonnewald U, et al. 2011.** Systems Analysis of a Maize Leaf Developmental Gradient Redefines the Current C₄ Model and Provides Candidates for Regulation. *Plant Cell* **23**(12): 4208-4220.
- Pignon CP, Jaiswal D, McGrath JM, Long SP. 2017.** Loss of photosynthetic efficiency in the shade. An Achilles heel for the dense modern stands of our most productive C₄ crops? *Journal of Experimental Botany* **68**(2): 335-345.
- Quirk J, Bellasio C, Johnson DA, Osborne CP, Beerling DJ. 2018.** C₄ savanna grasses fail to maintain assimilation in drying soil under low CO₂ compared with C₃ trees despite lower leaf water demand. *Functional Ecology* doi:10.1111/1365-2435.13240(00): 1-11.
- Retta M, Ho QT, Yin X, Verboven P, Berghuijs HNC, Struik PC, Nicolai BM. 2016.** A two-dimensional microscale model of gas exchange during photosynthesis in maize (*Zea mays* L.) leaves. *Plant Science* **246**(Supplement C): 37-51.
- Rogers A, Medlyn BE, Dukes JS, Bonan G, Caemmerer S, Dietze MC, Kattge J, Leakey ADB, Mercado LM, Niinemets Ü, et al. 2017.** A roadmap for improving the representation of photosynthesis in Earth system models. *New Phytologist* **213**(1): 22-42.
- Sage RF, Khoshravesh R. 2016.** Passive CO₂ concentration in higher plants. *Current Opinion in Plant Biology* **31**: 58-65.
- Sage TL, Sage RF. 2009.** The Functional Anatomy of Rice Leaves: Implications for Refixation of Photorespiratory CO₂ and Efforts to Engineer C₄ Photosynthesis into Rice. *Plant and Cell Physiology* **50**(4): 756-772.
- Sander R. 2015.** Compilation of Henry's law constants (version 4.0) for water as solvent. *Atmospheric Chemistry & Physics* **15**(8): 4399-4981.
- Schlüter U, Bräutigam A, Droz J-M, Schwender J, Weber AP.** The role of alanine and aspartate aminotransferases in C₄ photosynthesis. *Plant Biology* **0**(ja).
- Schlüter U, Denton AK, Bräutigam A. 2016.** Understanding metabolite transport and metabolism in C₄ plants through RNA-seq. *Current Opinion in Plant Biology* **31**: 83-90.
- Schmitt MR, Edwards GE. 1981.** Photosynthetic Capacity and Nitrogen Use Efficiency of Maize, Wheat, and Rice: A Comparison between C₃ and C₄ Photosynthesis. *Journal of Experimental Botany* **32**(3): 459-466.
- Sheehy JE, ed. 2007.** *Charting New Pathways to C₄ Rice*. Singapore: World Scientific Publishing.
- Snaydon RW. 1991.** The Productivity of C₃ and C₄ Plants - a Reassessment. *Functional Ecology* **5**(3): 321-330.
- Song Q, Zhang G, Zhu X-G. 2013.** Optimal crop canopy architecture to maximise canopy photosynthetic CO₂ uptake under elevated CO₂ – a theoretical study using a mechanistic model of canopy photosynthesis. *Functional Plant Biology* **40**(2): 108-124.
- Sowiński P 2013.** Characteristics of Symplasmic Transport. In: Sokołowska K, Sowiński P eds. *Symplasmic Transport in Vascular Plants*: Springer New York, 1-39.
- Sowinski P, Szczepanik J, Minchin PEH. 2008.** On the mechanism of C₄ photosynthesis intermediate exchange between Kranz mesophyll and bundle sheath cells in grasses. *Journal of Experimental Botany* **59**(6): 1137-1147.
- Sun W, Ubierna N, Ma J-Y, Walker B, Kramer D, Cousins AB. 2014.** The coordination of C₄ photosynthesis and the CO₂ concentrating mechanism in *Zea mays* and *Miscanthus × giganteus* in response to transient changes in light quality. *Plant Physiology* **164**(3): 1283-1292.
- Takeuchi Y, Akagi H, Kamasawa N, Osumi M, Honda H. 2000.** Aberrant chloroplasts in transgenic rice plants expressing a high level of maize NADP-dependent malic enzyme. *Planta* **211**(2): 265-274.
- Taylaran RD, Ozawa S, Miyamoto N, Ookawa T, Motobayashi T, Hirasawa T. 2009.** Performance of a High-Yielding Modern Rice Cultivar Takanari and Several Old and New Cultivars Grown with and without Chemical Fertilizer in a Submerged Paddy Field. *Plant Production Science* **12**(3): 365-380.
- Taylor SH, Hulme SP, Rees M, Ripley BS, Ian Woodward F, Osborne CP. 2010.** Ecophysiological traits in C₃ and C₄ grasses: a phylogenetically controlled screening experiment. *New Phytologist* **185**(3): 780-791.
- Tazoe Y, Hanba YT, Furumoto T, Noguchi K, Terashima I. 2008.** Relationships between quantum yield for CO₂ assimilation, activity of key enzymes and CO₂ leakiness in *Amaranthus cruentus*, a C₄ dicot, grown in high or low light. *Plant and Cell Physiology* **49**(1): 19-29.
- Ubierna N, Sun W, Cousins AB. 2011.** The efficiency of C₄ photosynthesis under low light conditions: assumptions and calculations with CO₂ isotope discrimination. *Journal of Experimental Botany* **62**(9): 3119-3134.
- Ubierna N, Sun W, Kramer DM, Cousins AB. 2013.** The Efficiency Of C₄ Photosynthesis Under Low Light Conditions In *Zea mays*, *Miscanthus X giganteus* And *Flaveria bidentis*. *Plant, Cell & Environment* **36**: 365-381.
- Violet-Chabrand S, Matthews JSA, Brendel O, Blatt MR, Wang Y, Hills A, Griffiths H, Rogers S, Lawson T. 2016.** Modelling water use efficiency in a dynamic environment: An example using *Arabidopsis thaliana*. *Plant Science* **251**: 65-74.
- Vollmar M, Schlieper D, Winn M, Büchner C, Groth G. 2009.** Structure of the c14 Rotor Ring of the Proton Translocating Chloroplast ATP Synthase. *Journal of Biological Chemistry* **284**(27): 18228-18235.
- von Caemmerer S. 1989.** A model of photosynthetic CO₂ assimilation and carbon-isotope discrimination in leaves of certain C₃-C₄ intermediates. *Planta* **178**(4): 463-474.
- von Caemmerer S. 2000.** *Biochemical models of leaf Photosynthesis*. Collingwood: CSIRO Publishing.
- von Caemmerer S, Furbank RT. 2003.** The C₄ pathway: an efficient CO₂ pump. *Photosynthesis Research* **77**(2-3): 191-207.

- Wang P, Kelly S, Fouracre JP, Langdale JA. 2013.** Genome-wide transcript analysis of early maize leaf development reveals gene cohorts associated with the differentiation of C4 Kranz anatomy. *The Plant Journal* **75**(4): 656-670.
- Wang S, Tholen D, Zhu X-G. 2017.** C4 photosynthesis in C3 rice: a theoretical analysis of biochemical and anatomical factors. *Plant, Cell & Environment* **40**(1): 80-94.
- Wang Y, Bräutigam A, Weber APM, Zhu X-G. 2014.** Three distinct biochemical subtypes of C4 photosynthesis? A modelling analysis. *Journal of Experimental Botany* **65**(13): 3567-3578.
- Warneck P, Williams J 2012.** Rate Coefficients for Gas-Phase Reactions. *The Atmospheric Chemist's Companion*: Springer, 227-269.
- Way DA, Oren R, Kim HS, Katul GG. 2011.** How well do stomatal conductance models perform on closing plant carbon budgets? A test using seedlings grown under current and elevated air temperatures. *Journal of Geophysical Research: Biogeosciences (2005–2012)* **116**(G4).
- Weber APM, von Caemmerer S. 2010.** Plastid transport and metabolism of C3 and C4 plants — comparative analysis and possible biotechnological exploitation. *Current Opinion in Plant Biology* **13**(3): 256-264.
- Wei J-C, Wang R-L, Cheng G-Y. 1994.** Studies on the kinetic properties of ribulose-1, 5-bisphosphate carboxylase from of F1 hybrid rice. *Acta Phytophysiologica Sinica* **20**: 55-60.
- Wu A, Doherty A, Farquhar GD, Hammer GL. 2017.** Simulating daily field crop canopy photosynthesis: an integrated software package. *Functional Plant Biology* **45**(3): 362-377.
- Yamori W, Shikanai T. 2016.** Physiological Functions of Cyclic Electron Transport Around Photosystem I in Sustaining Photosynthesis and Plant Growth. *Annual review of plant biology* **67**(1): 81-106.
- Yin X, Struik PC. 2015.** Constraints to the potential efficiency of converting solar radiation into phytoenergy in annual crops: from leaf biochemistry to canopy physiology and crop ecology. *Journal of Experimental Botany* **66**(21): 6535-6549.
- Yin X, Struik PC. 2017.** Can increased leaf photosynthesis be converted into higher crop mass production? A simulation study for rice using the crop model GECROS. *Journal of Experimental Botany* **68**(9): 2345-2360.
- Yin X, Struik PC, Romero P, Harbinson J, Evers JB, Van Der Putten PEL, Vos JAN. 2009.** Using combined measurements of gas exchange and chlorophyll fluorescence to estimate parameters of a biochemical C3 photosynthesis model: a critical appraisal and a new integrated approach applied to leaves in a wheat (*Triticum aestivum*) canopy. *Plant, Cell & Environment* **32**(5): 448-464.
- Yin X, van der Putten PEL, Driever SM, Struik PC. 2016.** Temperature response of bundle-sheath conductance in maize leaves. *Journal of Experimental Botany* **67**(9): 2699-2714.
- Yin XY, Struik PC. 2012.** Mathematical review of the energy transduction stoichiometries of C4 leaf photosynthesis under limiting light. *Plant Cell and Environment* **35**(7): 1299-1312.

Tables.

Table 1. Acronyms, definitions, values, and units used.

Symbol / Acronym	Definition	Values / Units	Source
A	Net assimilation	$\mu\text{mol m}^{-2} \text{s}^{-1}$	output
a_t	Total concentration of adenylates in chloroplast	12.7 mmol m^{-2}	Farquhar and Wong (1984)
BS	Bundle sheath		
C_{BS}	CO_2 concentration in the BS	$\mu\text{mol mol}^{-1}$	output
CCM	Carbon concentrating mechanism		
CEF	Cyclic electron flow		
C_M	CO_2 concentration in the M	$\mu\text{mol mol}^{-1}$	variable, iteratively found
D_S	Leaf to boundary layer water mole fraction gradient in the light ($10 \times \text{VPD}$ in kPa)	10 mmol $\text{H}_2\text{O mol air}^{-1}$	gas exchange
D_{S0}	Leaf to boundary layer water mole fraction gradient in the dark ($10 \times \text{VPD}$ in kPa)	8.6 mmol $\text{H}_2\text{O mol air}^{-1}$	gas exchange
E_t	Total concentration of Rubisco sites	6.7 mmol m^{-2}	adjusted from Farquhar and Wong (1984) by fitting gas exchange data
$f_{\text{C Rubisco}}$	Parameter defining the fraction of actual Rubisco carboxylation in BS relative to leaf-level	dimensionless	set to equal $V_{\text{CBS}}/V_{\text{C}}$ output of the enzyme-limited model
f_{Cyc}	Fraction of J_1 following CEF	dimensionless	fitted to max A
f_{NDH}	Fraction of CEF through the NDH complex	0 (C_3 and C_2); 0.2 and 0± (C_2+C_4); 0.4 and 0± (C_4)	assigned
f_{PPDK}	Parameter defining the fraction of PPDK activity in the BS relative to leaf-level	0	assigned
$f_{\text{PR}}, f_{\text{CS}}$	Parameter defining the fraction of activity in BS relative to leaf-level, of phosphoglycerate reduction rate, and carbohydrate synthesis	0 (variable for the simulations of Figure 6B and 6D)	assigned
$f_{\text{Pseudocyc}}$	Fraction of J_1 following used by alternative sinks of electrons like nitrate reduction and the water-water cycle	0.1	assigned (Yin & Struik, 2012)
f_{Q}	Fraction of J_1 going through the Q-Cycle	1	Yin and Struik (2012)
f_{RLIGHT}	parameter defining the fraction of respiration in the light in BS relative to leaf-level	0 (C_3); 0.2 (C_2); 0.5 (C_2+C_4 , and C_4)	(von Caemmerer, 1989; von Caemmerer, 2000)
g_{BS}	Bundle sheath conductance to CO_2 diffusion	0.00287† mol $\text{m}^{-2} \text{s}^{-1}$	Yin <i>et al.</i> (2016)
GDC	Glycine decarboxylase		
g_M	Mesophyll conductance to CO_2 diffusion	0.26† mol $\text{m}^{-2} \text{s}^{-1}$	gas exchange
g_{S0}	Stomatal conductance in the dark	0.047 mol $\text{CO}_2 \text{m}^{-2} \text{s}^{-1}$	gas exchange
h	Stoichiometry of ATP synthase: protons required to synthesize ATP	4.67 protons / ATP	Vollmar <i>et al.</i> (2009); Hahn <i>et al.</i> (2018)
$l, l_1, l_2, l_{10}, l_{20}$	Light absorbed by PSI and PSII, by PSI, by PSII, by PSI when $f_{\text{Cyc}}=0$, by PSII when $f_{\text{Cyc}}=0$, respectively	$\mu\text{mol m}^{-2} \text{s}^{-1}$	output
J_1, J_2	Electron flow through PSI, and PSII, respectively	$\mu\text{mol m}^{-2} \text{s}^{-1}$	output
J_{ATP}	Total leaf-level ATP production rate	$\mu\text{mol m}^{-2} \text{s}^{-1}$	output
J_{NADPH}	Total leaf-level NADPH production rate	$\mu\text{mol m}^{-2} \text{s}^{-1}$	output
J_{SAT}	PPFD saturated electron transport rate	310† $\mu\text{mol m}^{-2} \text{s}^{-1}$	chlorophyll fluorescence
K_{C}	Rubisco Michaelis-Menten constant for CO_2 in the liquid phase	8† μM	(Wei <i>et al.</i> , 1994; von Caemmerer, 2000; Galmés <i>et al.</i> , 2016; Hermida-Carrera <i>et al.</i> , 2016)
K_n	Effective hydraulic conductance from the soil to the epidermis	12 mmol $\text{H}_2\text{O m}^{-2} \text{s}^{-1} \text{MPa}^{-1}$	Bellasio <i>et al.</i> (2017)
Kh_{CO_2}	volatility of CO_2	30.3† $\mu\text{bar } \mu\text{M}^{-1}$	Sander (2015)
Kh_{O_2}	volatility of O_2	833.3† $\mu\text{bar } \mu\text{M}^{-1}$	Warneck and Williams (2012)
K_o	Rubisco Michaelis-Menten constant for O_2 in the liquid phase	335† μM	von Caemmerer (2000)
M	Mesophyll		
NDH	NAD(P)H Dehydrogenase-like (complex)		
O_M, O_{BS}	O_2 concentration in M cells or BS cells	O_M is 210000 or 21000 $\mu\text{mol mol}^{-1}$ O_{BS} is calculated	O_M is assigned O_{BS} is output
p	Concentration of photophosphorylation sites	7.5 mmol m^{-2}	adjusted from Farquhar and Wong (1984) by fitting gas exchange data
PEPC	Phosphoenolpyruvate carboxylase		
PEPCK	Phosphoenolpyruvate carboxykinase		
PPDK	Pyruvate phosphate dikinase		

<i>PPFD</i>	Photosynthetic photon flux density	$\mu\text{mol m}^{-2} \text{s}^{-1}$	assigned
R_{LIGHT} , $R_{\text{LIGHT BS}}$, $R_{\text{LIGHT M}}$	Respiration in the light, leaf-level, in the BS or in the M, respectively	R_{LIGHT} is $0.8\ddagger \mu\text{mol m}^{-2} \text{s}^{-1}$	gas exchange, 0.5 is the assumed fraction of BS respiration relative to total assigned
r_{PEPCK}	input parameter defining the activity of PEPCK relative to V_P	0	assigned
Rubisco	Ribulose biphosphate carboxylase oxygenase		
RuBP	Ribulose-1,5-bisphosphate		
s	lumped energy conversion coefficient (Yin <i>et al.</i> , 2009)	$0.38 \text{ e}^-/\text{quanta}$	gas exchange
$S_{\text{C/O}}$	Rubisco specificity	$2800\ddagger \mu\text{bar}/\mu\text{bar}$ (gas) or $102\ddagger \text{mol mol}^{-1}$ (liq)	gas exchange
$V_{\text{C MAX}}$, V_{C} , $V_{\text{C BS}}$, $V_{\text{C M}}$	Rubisco carboxylation rate, CO_2 saturated, leaf-level, in the BS, in the M, respectively	$V_{\text{C MAX}}$ is $93\ddagger \mu\text{mol m}^{-2} \text{s}^{-1}$	$V_{\text{C MAX}}$ by gas exchange, or output
V_{O} , $V_{\text{O BS}}$, $V_{\text{O M}}$	Rubisco oxygenation rate, total, in the BS or in the M, respectively	$\mu\text{mol m}^{-2} \text{s}^{-1}$	output
$V_{\text{P(J)}}$	Leaf-level actual phospho $enol$ /pyruvate carboxylation rate, inputs to the light-limited model	0 (C_3 and C_2); $0.075J_{\text{ATP}}$ (C_2+C_4); $0.2J_{\text{ATP}}$ (C_4) $\mu\text{mol m}^{-2} \text{s}^{-1}$ (variable for the simulations in Figure 6)	assigned (von Caemmerer, 2000)
$V_{\text{P MAX}}$	CO_2 saturated phospho $enol$ /pyruvate carboxylation rate	0 (C_3 and C_2); $0.1J_{\text{SAT}}$ (C_2+C_4); $0.3J_{\text{SAT}}$ (C_4) $\mu\text{mol m}^{-2} \text{s}^{-1}$	assigned
V_r	Potential pool size of RuBP	150 mmol m^{-2}	Farquhar and Wong (1984)
$Y(I)_{\text{LL}}$	Yield of PSI extrapolated under zero <i>PPFD</i>	1	Yin and Struik (2012)
$Y(II)_{\text{LL}}$	Yield of PSII extrapolated under zero <i>PPFD</i>	0.75	chlorophyll fluorescence
$Y(II)_{\text{MOD}}$	Yield of PSII modelled empirically by a non-rectangular hyperbola	dimensionless	output
α	parameter scaling BS O_2 evolution to net assimilation attributed to BS activity	1	von Caemmerer (1989)
Y^*	Half the reciprocal Rubisco specificity $\gamma^* = \frac{1}{2S_{\text{C/O}}}$	dimensionless	output
θ	Curvature of the non-rectangular hyperbola used to model the light-dependence of $Y(II)$	0.5	gas exchange
θ_A	Curvature of the non-rectangular hyperbola used to smooth the combination of light-limited and enzyme-limited models	0.95	Buckley <i>et al.</i> (2016)
ξ_{GDC}	Specifies the fraction of V_{OM} which is decarboxylated in the BS.	0 (C_3) and 1 (C_2 , C_2+C_4 , and C_4)	Sage and Khoshravesh (2016)
χ_I	Fraction of I shifting from PSII to PSI upon engagement of CEF	dimensionless	output
χ_{Rubisco}	parameter defining the fraction of $V_{\text{C MAX}}$ in BS relative to leaf-level	dimensionless	fitted to maximise A
$\chi_s\beta$	Parameter lumping turgor to conductance scaling factor and the hydromechanical / biochemical response parameter	$0.055 \text{ mol air mmol}^{-1} \text{ ATP s}^{-1} \text{ MPa}^{-1}$	fitted to gas exchange data
ψ_{Soil} , ψ_{Soil0}	Soil water potential in the light or in the dark respectively	0 MPa	assigned
π_e	Epidermal osmotic pressure	1.2 MPa	Bellasio <i>et al.</i> (2017)

† The value shown is at 25 °C but the quantity was made temperature-dependent; ‡ Alternative scenarios in Figure 4

Figures.

Figure 1. Modelling framework. Blue boxes show inputs while orange boxes show outputs; grey boxes represent submodels. Inputs with a thick blue outline are made temperature-dependent. Submodels contoured in red are originally developed for this work. Photosynthetic photon flux density ($PPFD$) is an input to the electron transport submodel to calculate the total ATP production rate (J_{ATP}) and the total NADPH production rate (J_{NADPH}). These and dummy values for CO_2 concentration at the M carboxylating sites (C_M) are fed into the light- and enzyme-limited submodels (Dashed boxes). The outputs from the photosynthesis submodels are used to calculate chloroplastic ATP concentration (τ) and a smoothed combination of the submodels is fed into a stoichiometric submodel to calculate fluxes and reaction rates. τ is used in the stomatal submodel along with inputs for soil water potential (Ψ_{Soil}) and evaporative demand (D_s). The output stomatal conductance (g_s) is used to calculate CO_2 concentration in the sub-stomatal cavity (C_i) from external CO_2 concentration (C_a) and in turn used to calculate C_M , which is iterated. See Table 1 for more abbreviations.

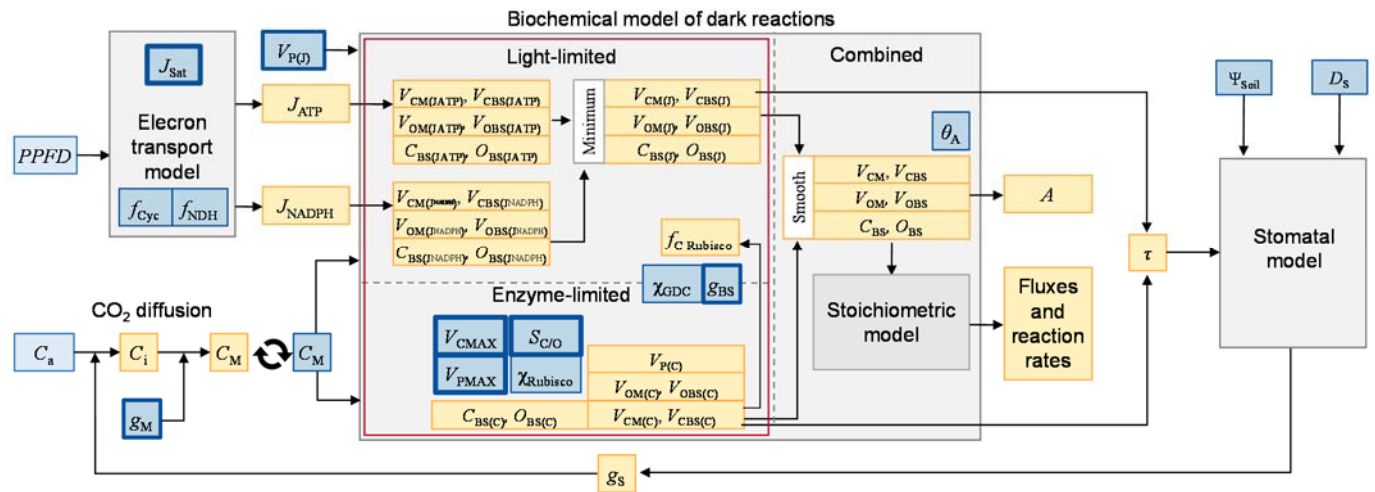


Figure 2. Assimilation and stomatal conductance measured on rice and corresponding simulations for a C_3 photosynthetic type. Panel **A**: light–response curves. Symbols show the response of A to decreasing $PPFD$ measured under ambient O_2 (closed circles) or 2% O_2 (open circles). Lines show modelled assimilation under ambient O_2 (solid line) or 2% O_2 (dashed line). Panel **B**: A/C_i curves. Symbols show the measured A at varying levels of CO_2 concentration in the substomatal cavity, C_i , under ambient and low O_2 . Lines show the corresponding simulations. Panel **C**: measured and simulated response of stomatal conductance (g_s) to $PPFD$ under ambient and low O_2 . Panel **D**: measured and simulated response of stomatal conductance (g_s) to external CO_2 concentration, C_a , under ambient and low O_2 . Symbols show mean \pm SE, $n=4$. For simulated A/C_i curves, C_a was set at 16 levels [between 20 and 1000 $\mu\text{mol mol}^{-1}$] while $PPFD$ was set at 1200 $\mu\text{mol m}^{-2} \text{s}^{-1}$, the same used for gas exchange measurements. For simulated $A/PPFD$ curves, $PPFD$ was set at 18 levels [between 1 and 1500 $\mu\text{mol m}^{-2} \text{s}^{-1}$] and C_a was set at 400 $\mu\text{mol mol}^{-1}$. Temperature was 25° C while χ_{Rubisco} and f_{Cyc} were fitted for each combination of inputs.

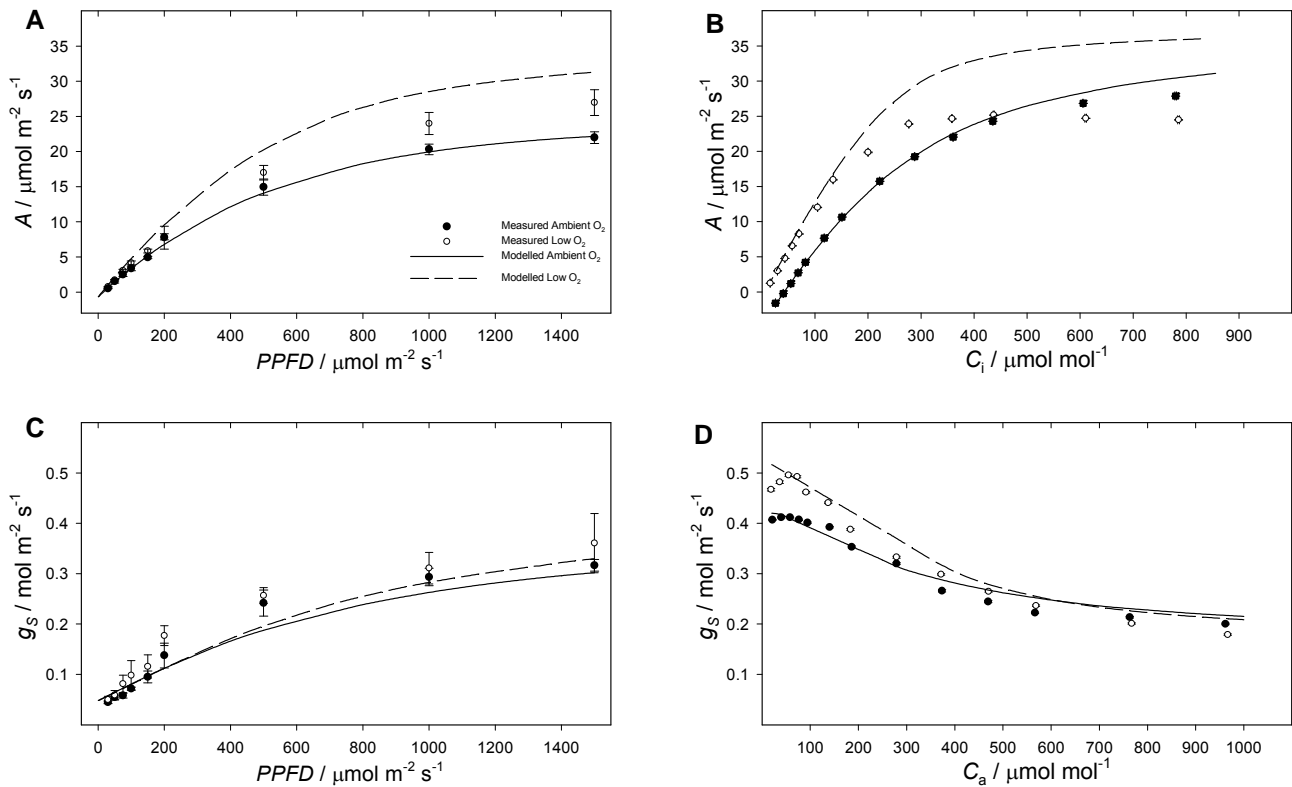


Figure 3. Simulated A -response curves. Compared model output for the four photosynthetic types in response to changes in $PPFD$ (Left) or C_a (Right) varied in the same steps of curves above. Four different photosynthetic types were simulated in a best case scenario for bioengineering whereby NDH is expressed ($f_{NDH} > 0$), $f_{C_{Yc}}$ and $\chi_{Rubisco}$ are optimal (fitted to max A): C_3 (black solid line), representing the measured plants; C_2 (orange dashed line); C_2+C_4 (red solid line); and C_4 (blue dash-dot line). Panels **A** and **B**: net assimilation. Panels **C** and **D**: stomatal conductance. Panels **E** and **F**: CO_2 concentration in the BS. Panels **G** and **H**: Rubisco rate of oxygenation to carboxylation V_o/V_c . Panels **I** and **J**: fraction of Rubisco carboxylating activity in the BS, relative to total.

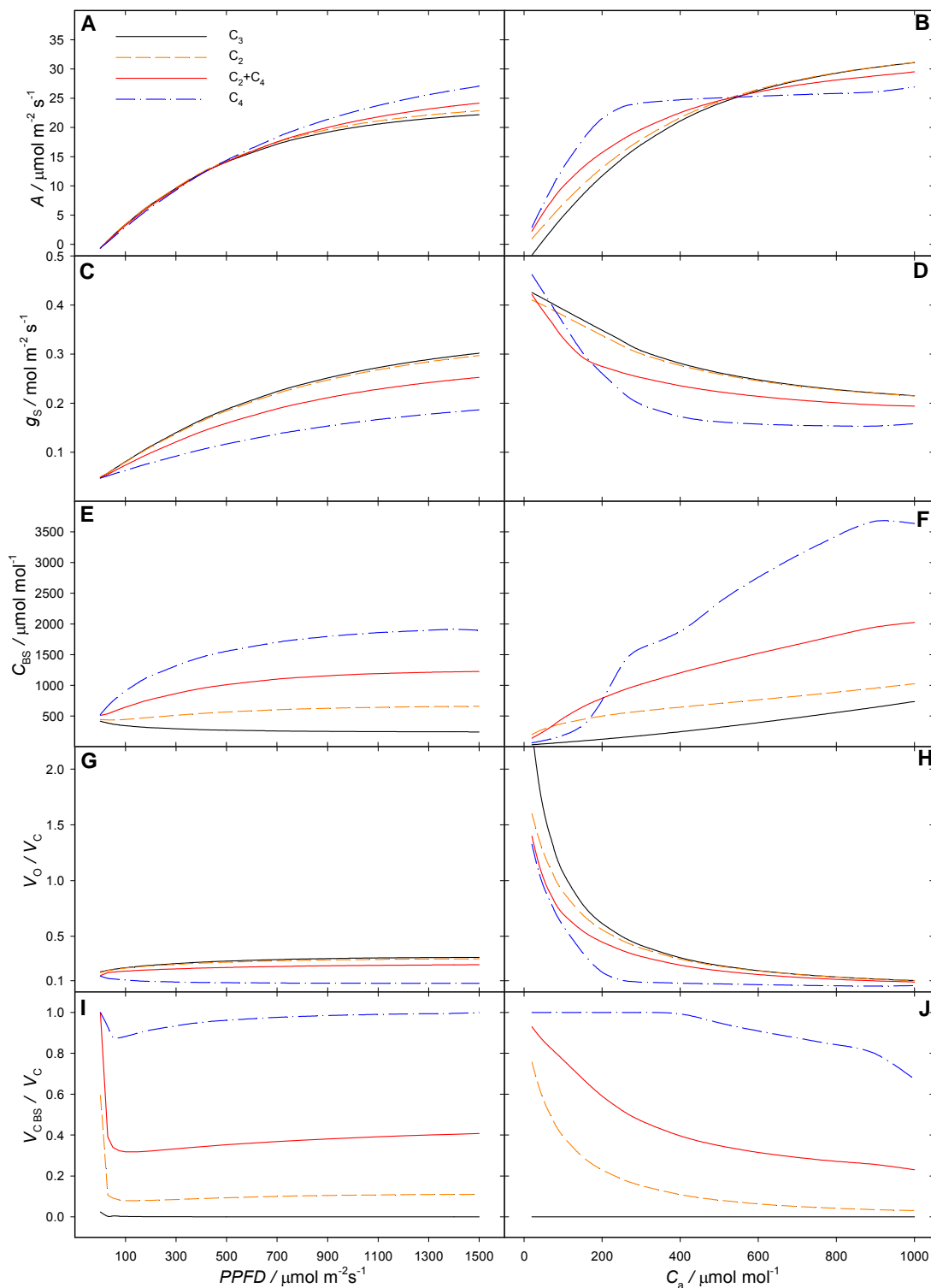


Figure 4. Assimilation in the best case scenario. Gains were calculated for 100 combinations of temperature (varied in 10 steps from 16 °C to 43 °C) and *PPFD* (varied in 10 steps from 1 to 1500 $\mu\text{mol m}^{-2} \text{s}^{-1}$), under a C_a of 400 $\mu\text{mol mol}^{-1}$ (top row), or in 100 combinations of C_a (varied in 10 steps from 150 to 690 $\mu\text{mol mol}^{-1}$) and temperature (as above), under a *PPFD* of 700 $\mu\text{mol m}^{-2} \text{s}^{-1}$ (bottom row) in a best case scenario whereby electron transport processes fully accommodate for the presence of different types of CCM ($f_{\text{NDH}} > 0$, f_{Cyc} is fitted) and Rubisco is optimally allocated (χ_{Rubisco} is fitted). The gain was expressed as relative to C_3 assimilation (Panels **A** and **E**), for C_2 (Panel **B** and **F**) C_2+C_4 (panel **C** and **G**) and C_4 (panel **D** and **H**).

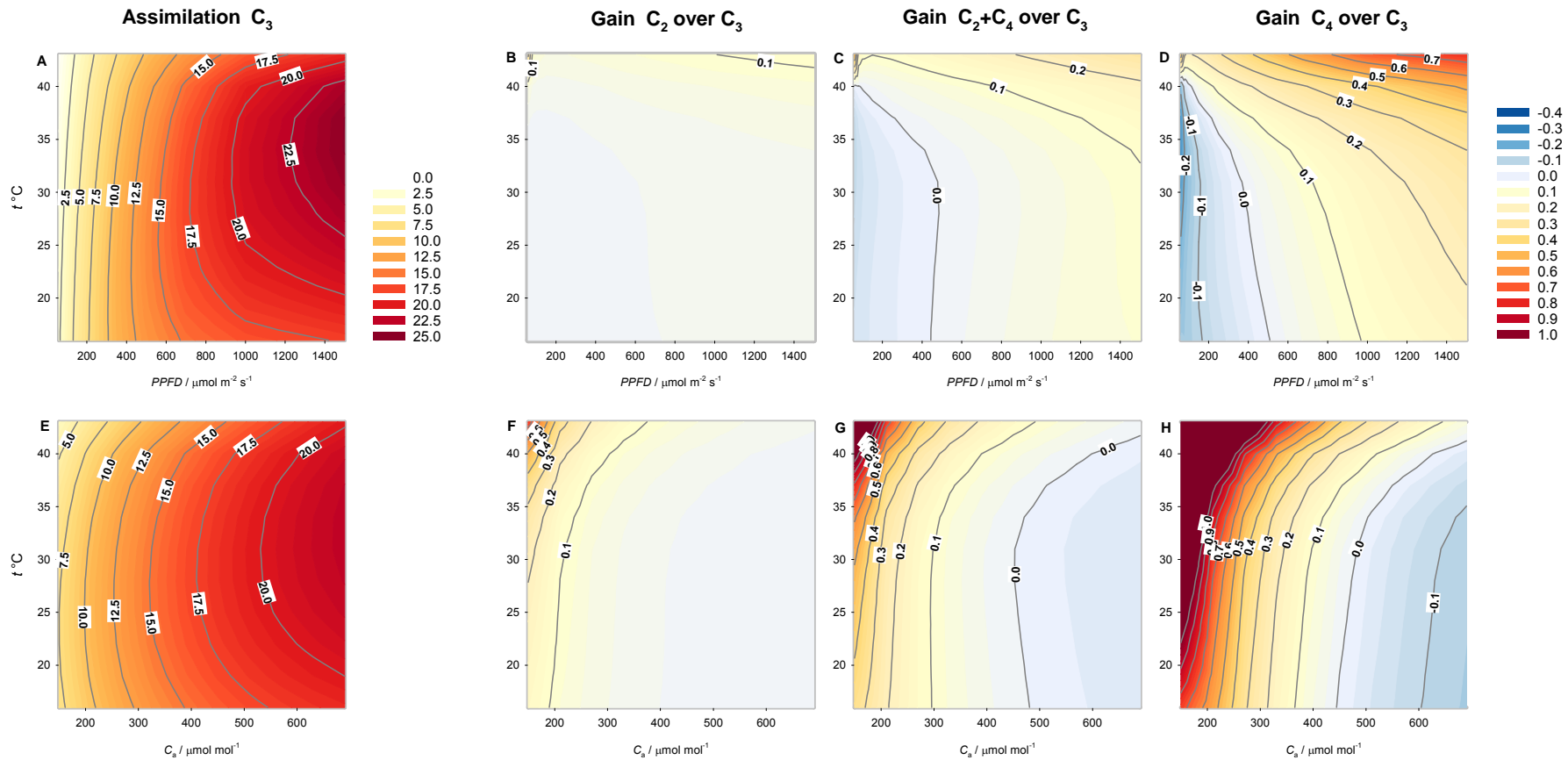


Figure 5. Assimilation in alternative scenarios. Gains were calculated in the temperature \times *PPFD* space, under a C_a of $400 \mu\text{mol mol}^{-1}$, expressed as relative to C_3 assimilation (Figure 4). Panels **A**, **B**, and **C** show a less optimistic scenario whereby the activity of the NDH complex remain at C_3 levels, modelled by setting f_{NDH} at zero for all photosynthetic types. Panels **D**, **E** and **F** show a pessimistic scenario whereby in addition to $f_{\text{NDH}}=0$, the fraction of cyclic electron flow (f_{Cyc}) was set at C_3 levels for all photosynthetic types.

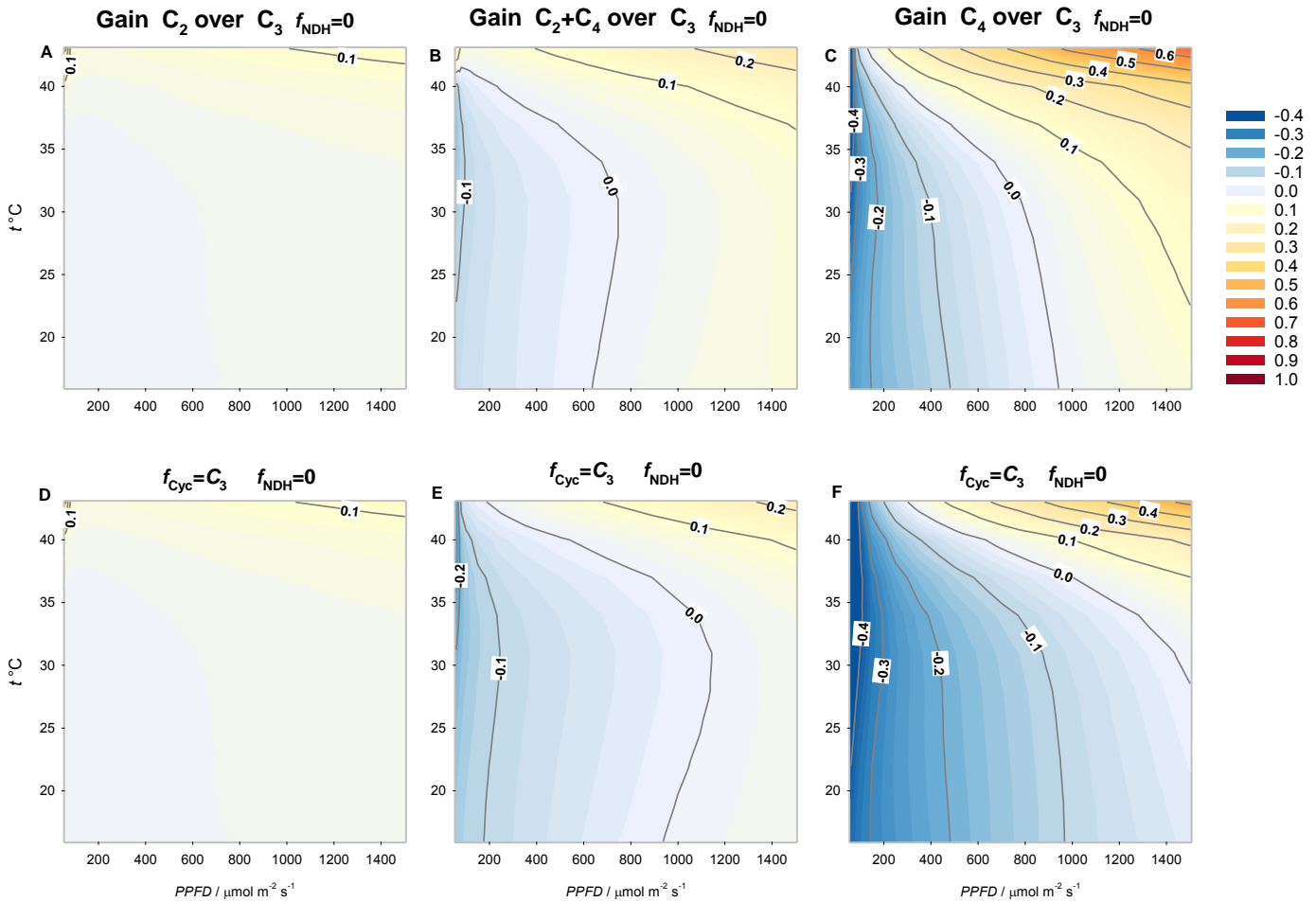


Figure 6. Modelled fluxes between the M and the BS at increasing levels of C₄ engagement. In this simulation the C₄ CCM was increasingly upregulated by manipulating PEPC activity ($V_{P(J)}$, $\mu\text{mol m}^{-2} \text{s}^{-1}$) to increase from 0 to $0.2 J_{ATP}$ to represent the C₂ to C₄ continuum (from left to right of each panel). Panel **A** simulates a scenario of minimum ATP demand in BS obtained by setting r_{PEPCK} , f_{PR} , f_{CS} and f_{PPDK} at zero; other inputs represented the operational conditions of $PPFD$ $700 \mu\text{mol m}^{-2} \text{s}^{-1}$, 25°C , and $C_a=350 \mu\text{mol mol}^{-1}$. Panel **B** simulates a scenario of minimum sum of squared flow rates between BS and M obtained by fitting f_{PR} , and f_{CS} . In these conditions the ATP demand in BS increased substantially, and is shown as relative to the ATP demand in the M in panels **C** and **D**. The flux is considered positive when in the M to BS direction for MAL, ASP, DHAP, and GLY, and in the opposite direction for the other metabolites (Figure S1). Note the different scaling of y-axes.

